POLITECNICO DI MILANO

Scuola di Ingegneria Industriale e dell'Informazione

Corso di Laurea Magistrale in Ingegneria Elettrica

RESEARCH ON MUTUAL FEEDBACK AC DRIVE TEST SYSTEM BASED ON REPETITIVE CONTROL

Relatore: Prof. Enrico Ragaini

Correlatore: Prof. Guochun Xiao

Tesi di Laurea Magistrale di:
Shuai Su
Matr. 854628

Anno Accademico 2017-2018

CONTENTS

LIST OF FIGURES

LIST OF TABLES

SOMMARIO

Negli ultimi anni, lo studio riguardo la locomotiva elettrica ha suscitato grande attenzione dei ricercatori. A causa delle caratteristiche, come ad esempio la struttura complessa e l'elevato costo tipica delle locomotive elettriche, tutto ciò ha reso con una difficoltà piuttosto alta nella simulazione sulla caratteristica esecutiva della macchina reale. Il presente elaborato ha creato una piattaforma sperimentale ad alimentazione reciproca di piccola potenza attraverso la tecnica del raddrizzatore PWM e la tecnica di controllo vettoriale, per simulare con esattezza le caratteristiche esecutive del modello HXD3 della locomotiva elettrica. Perciò è necessario creare un dispositivo di monitoraggio con funzioni complete nel sistema sperimentale dell'azionamento AC.

Il presente elaborato presenta il principio di funzionamento e il modello matematico del raddrizzatore PWM monofase, procedendo poi con lo studio sulle tattiche di controllo di tale raddrizzatore. Sono passato poi alla progettazione del regolatore per le 3 tattiche di controllo, quello del PI, quello della risonanza proporzionale e quello controllo ripetitivo, e alla successiva verifica di stabilità, analizzando i pregi e i difetti di queste tre tattiche di controllo, alla fine il banco di prova ha deciso di utilizzare la tattica del controllo ripetitivo ottenendo un'ottimo effetto di controllo.

In seguito, ho fatto la presentazione del modello matematico di motore asincrono, per il problema della difficoltà nella sua regolazione di velocità, è stata utilizzata la tecnica di controllo vettoriale orientato verso il campo magnetico rotante, la velocità e la catena magnetica del motore asincrono ottiene il disaccoppiamento totale, sulla base di questi è stata completata la progettazione del regolatore di motore, procedendo poi alla verifica della stabilità dei regolatori.

Il presente elaborato, sulla base della piattaforma di simulazione Matlab/Simulink, procede poi alla verifica di simulazione verso il banco di prova dell'azionamento AC ad alimentazione reciproca, completando la costruzione della piattaforma per il sistema sperimentale dell'azionamento AC sopra citato, portando al termine l'esperimento con il nucleo di comando TMS320F28335DSP.

Il presente elaborato si è basato sulla tecnica della linea generale CAN e sulla tecnica di comunicazione RS485 per creare un sistema di monitoraggio di alta stabilità e di funzione completa.

ABSTRACT

Research on electric locomotives in recent years has attracted widespread attention. Due to the complex structure and high cost of electric locomotives, it is difficult to simulate the operating characteristics of actual locomotives. Therefore, this paper builds a low-power mutual feedback AC drive test platform to accurately simulate the operating characteristics of the HXD_3 electric locomotive. In addition, the control system of the AC drive test platform is complex and has high requirements on the power quality and the control accuracy. Therefore, it is necessary to develop a monitoring device with perfect function in the AC drive test system.

Firstly, this paper introduces the working principle and mathematical model of single-phase PWM rectifier. Three controllers of PI control, PR control and repetitive control are designed and tested. The advantages and disadvantages of the three control strategies are analysed and verified. Lastly the repetitive control is adopted.

Then this paper introduces the mathematical model of asynchronous motors. In view of the difficulty in speed regulation of asynchronous motors, vector control technique based on rotor magnetic field orientation is adopted to realize the complete decoupling of the speed and flux linkage of asynchronous motors. The design of the flux linkage controller and the speed controller are completed and the stability of the controllers is verified.

Then the mutual feedback AC drive test platform is verified by Matlab/Simulink simulation platform. The experiment is completed with the TMS320F28335 DSP as the control core. The single-phase PWM rectifier based on repetitive control, vector control system based on rotor magnetic field orientation, and verification of energy feedback of the whole system are completed. Besides, the correctness of the above control system design is proved.

Finally, this paper presents the overall design of the monitoring device with accurate monitoring and strong anti-interference capability based on the CAN bus communication technology and RS485 communication technology.

1 INTRODUCTION

With the vigorous development of the transportation industry, the demand for functions of electric locomotive has also increased. The HXD_3 electric locomotive is the main electric locomotive model for Chinese railways. Due to the complex structure, high power consumption and high cost of electric locomotives, it is difficult to simulate the operating characteristics of actual locomotives. However, with the improvement of power electronics and the richness of communication methods, research on AC drive test system has also come to a new stage. At the same time, a fully functional AC drive test system has high requirements for power quality, system stability, speed control capability, energy feedback indicators, and monitoring devices.

Traditional rectifiers often generate harmonic currents and reactive power on the grid side, affecting power quality and normal operation of load devices. Induction motors have the advantages of high efficiency, light weight, simple structure, reliable operation, and easy maintenance and are widely used in the traction link of electric locomotives. However, its speed control is complex and difficult; the control system of the mutual feedback AC drive test platform is complicated, which requires its monitoring device to achieve accurate observation, real-time monitoring and other functions.

1.1 Development and Research Status of Single-phase PWM Rectifier

With the rapid development of power electronics technology, power electronics converters such as rectifiers, inverters, and high-frequency switching power supplies have been widely used in power systems, chemicals, oil and gas, rail transit, metallurgy, port machinery, new energy, communications, home appliances and other industries. At present, most of these converter devices obtain the stable DC bus voltage through a rectifier circuit. The traditional rectification technology generally adopts uncontrolled rectification or

phased rectification, which will bring a large amount of current harmonics and reactive power to the power grid, causing serious grid pollution. Current harmonics will reduce the efficiency of energy production, transmission, and utilization. A large amount of current flowing through the neutral harmonics will overheat the circuit or even cause fire. Harmonic current will also affect the normal operation of electrical equipment. Vibration, noise, and overvoltage cause local overheating of the transformer, which results in aging of the insulation and reduced life of the electrical equipment. Harmonics may cause parallel resonance and series resonance of the power grid and increase the harm of harmonics. Harmonics cause malfunctions of relay protection and automatic device, as well as interference with nearby communication systems. The increase of reactive power will lead to increase of current, which will force the power capacity of electrical equipment and wires to increase; at the same time, the increase of the total current of the circuit will increase the loss of the equipment and the line; the reactive current will increase the voltage drop of the line and the transformer. The impact reactive power load will also cause the voltage to fluctuate violently, which will degrades the quality of the power supply. Therefore, current harmonics and reactive power have great harm to the power system. In order to meet the harmonic and reactive power standards, PWM rectifier technology can be applied.

PWM technology first appeared in the 60s of the 20th century. PWM technology achieves the goal of controlling output size by modulating the pulse width. Boris Mokrytski first proposed the combination of frequency control and PWM technology, and applied it to the control circuit of an AC motor [1]. This innovative method has a good suppression effect on the harmonic content of the output voltage, and makes the general inverter circuit have the function of variable voltage conversion. However, due to technical defects in semiconductor materials and power electronic devices, the technology has not achieved wide practical application. Since the 1980s, the semiconductor material industry has been booming, and the technology and performance of power switching devices have been continuously improved. People have also gained a deeper understanding of the application of PWM technology. With the optimization of the mathematical model of the single-phase PWM rectifier, the richness topology structure, the improvement of the control strategy and the progress of semiconductor material technology, the exploration of the single-phase PWM rectifier has also come to a new period. At the same time, the areas involved in

single-phase PWM rectifier technology are becoming increasingly widespread, such as new energy generation, uninterruptible power supplies, and AC drives. At present, the research on the single-phase PWM rectifier technology focuses on three aspects: the optimization of the mathematical model, the richness of the topological structure, and the improvement of the control strategy.

Establishing a mathematical model is the key to connect mathematical tools and solving practical engineering problems. Considering the equation of state of the voltage and current of the single-phase PWM rectifier in the unit switching period, literature [2] and literature [3] respectively deduce the mathematical model of the half-bridge single-phase PWM rectifier and the mathematical model of the full-bridge single-phase PWM rectifier. The literature [4] deduces the time domain model of the single-phase PWM rectifier under high frequency conditions based on the simplified state equations of voltage and current under high frequency conditions. Based on the average state equation, literature [5] establishes a linear time-invariant steady state and linear small-signal mathematical model of the single-phase PWM rectifier through linearization and elimination of time variables. This mathematical model can be applied to two-level and three-level topological structure.

Single-phase PWM rectifier can be classified according to many aspects. According to the circuit structure, it can be divided into half-bridge type and full-bridge type; according to the energy storage method of DC side，it can be divided into voltage source type and current source type; according to number of modulation levels，it can be divided into two -level type and three-level type.

With respect to the control of the single-phase PWM rectifier, on the one hand, the stable bus voltage on the DC side is required, and on the other hand, it is required to suppress the harmonic current on the AC side, and it is required that the AC side can realize unit power factor operation. The DC bus voltage can be controlled by controlling the input current on the AC side. Therefore, the control of the input current on the AC side is critical to the normal operation of the single-phase PWM rectifier. According to whether it directly controls the input current of the AC side, the control strategy of the single-phase PWM rectifier can be divided into direct current control and indirect current control.

The basic principle of the direct current control is: the command value of the input current of the AC side is corrected firstly, and unites the actual value of the input current to form a

closed-loop control, achieving the control target. In this feedback system, the reference value of the current is AC value, but the traditional PI control method cannot achieve the no-difference adjustment for the AC value control [6]. In order to improve the control performance, more and more control strategies have been applied to the research on single-phase PWM rectifiers. The literature [7] adopts the control strategy of repetitive control, which reduces the steady-state error of the system and improves the steady-state performance of the rectifier. The literature [8] adopts the control strategy of proportional resonance (PR) control to suppress the AC-side input current, which also decreases the steady-state error and significantly improves the response speed of the system. Literature [9] adopts a novel predictive current control strategy for multi-level rectifiers, reducing the switching frequency, reducing the switching losses, and optimizing the current waveform. In addition, control methods such as hysteretic loop control, neural network control, and adaptive control are increasingly being applied to the research on single-phase PWM rectifier. The rectifier with direct current control has good dynamic characteristics and high reliability. Compared with indirect current control, it has better performance. It is currently the main research direction of single-phase PWM rectifier [10]. This article adopts the control strategy of direct current control, which will be analysed in detail in the following sections.

The basic principle of indirect current control is to control the input current by controlling the input voltage on the AC side so that the phases of the input voltage and the input current are consistent [11]. For single-phase PWM rectifiers with indirect current control, current closed-loop control is no longer used. Instead, a voltage closed loop is constructed by the DC-side voltage. The output of the control loop is the input current amplitude of the AC side. The reference voltage of the resistance voltage on the AC side and the reference voltage of the inductor voltage can be obtained by the products between the output of the control loop and the sine and the cosine of the grid voltage angle respectively. At last, the modulation signal is obtained and then the ideal input current can be reached through SPWM modulation. Based on the traditional indirect current control strategy, literature [12] proposes a novel voltage loop control strategy based on sliding mode structure, which improves the stability of the rectifier and the speed of dynamic response. Literature [13] proposes a novel indirect current control strategy by adding a delay angle to the modulation signal of each phase, thereby simplifying the control system and improving the

system accuracy. In the indirect current control method, the AC-side input current does not need to be sampled in real time, so the current sensor can be saved in practical applications. In addition, this method also has the advantages of simple control, easy implementation, and simple structure. However, this method also has the disadvantages of slow dynamic response, sensitivity to changes in main circuit parameters, and lack of over-current protection.

1.2 Development and Research Status of the AC Drive System

1.2.1 Development of the AC Drive System

Electric traction is the top priority in the research of rail transit. Different from traditional steam engine traction and internal combustion engine traction, electric traction has gained more and more attention with its own excellent characteristics [14]. In accordance with the differences in the types of motors used in the AC drive system, the electric traction system is divided into two types: AC drive system and DC drive system.

Traction motor is the core component of energy conversion in the composition of electric locomotives. In the traction mode, the motor converts electrical energy into mechanical energy, which provides power for the operation of the electric locomotive; while in the braking mode of operation, the motor converts the mechanical energy of the locomotive into electrical energy and stores it in a certain way to provide the brake force of the locomotive. There are mainly four types of the traction motors: DC motors, AC asynchronous motors, permanent magnet motors, and switched reluctance motors [15]. These types of motors have their own advantages and disadvantages in terms of traction drive.

Due to its features such as easy speed control, simple control, and mature technology, DC motors have long been used in electric locomotive drives. In the 1970s, the traction drive technology of DC motors was fully mature. However, in the application of actual projects, the defects and disadvantages of DC motors are gradually exposed. The brush and commutator exist in the DC motor, and the mechanical structure is complex. It is prone to failure, and it is difficult to detect and maintain. Because of the inherently low efficiency, the locomotive has a low power factor and a narrow constant power range. So from the 1970s international researchers began to invest a lot of time and money into AC motor

drive research. In 1979, the first batch of E120 series high-power AC transmission locomotives in West Germany were successfully developed and put into use, indicating that AC drive technology has entered a new stage of development [16]. In the early 1990s, in the transportation fields of developed countries such as Europe and the United States, AC drive technology has become popular. Newly manufactured locomotives have already abandoned DC motor power devices.

There are two main types of AC traction drive technology: one is asynchronous motor drive technology, and the other is synchronous motor drive technology. Now the more widely used type is the asynchronous motor speed control. Synchronous motor drive technology applications are less and just promoted in the early stages by several European countries. This article adopts asynchronous motor drive technology. Because of its high efficiency, light weight, simple mechanical structure, stable operation and convenient maintenance, asynchronous motors overcome the inherent defects of DC motors from the structure of the motor and bring the traction drive technology into a new period of development. With the advancement of semiconductor material technology and power electronics technology, a large number of new types of power electronic devices emerge in an endless stream, and they have made great achievements in locomotive power supply and transmission systems, providing the basis for AC drive technology from the hardware field. With the rapid development of research on motor control technologies, vector control, direct torque control, and slip frequency control are increasingly used in traction drives. The rapid development of AC transmission technology has completed the high speed and heavy load of electric traction technology. Asynchronous motor has excellent traction braking characteristics and high adhesion utilization. Besides, it has the characteristics of high efficiency, small size, light weight, a wide range of constant power and so on, so it has been widely used. Because the AC drive technology can make the system power factor close to 1, with good regenerative braking performance, low maintenance cost, little interference with the communication function of the system, which promotes the trend of electric traction drive technology from DC drive technology to AC drive technology cannot be reversed [17-20].

1.2.2 Requirements of the AC Drive System

For railway traction, starting, speed regulation and braking are the basic rules of train operation and the basic requirements that the locomotive transmission system must meet.

In particular, the speed regulation of locomotives is the common basis for these three types of operating conditions. When hauling a train, the driver must adjust the speed of the locomotive according to different operating conditions. In order to give full play to the power of the locomotive, it is required that the motor can not only change the traction under different line and load conditions, but also require different speeds under the same traction conditions. It can be seen that the traction drive system of the locomotive must ensure that the torque and speed of the traction motor can be adjusted independently and have a wide adjustment range. When the locomotive is starting, it is expected that there will be a larger traction force to obtain a greater acceleration, thereby pulling the heavier train. However, the traction force of the motor is affected by many factors, such as the electrical characteristics of the traction motor itself, the excitation mode of the motor, the motor speed control method, the connection mode between the motors, the mechanical suspension mode, and the structure of the mechanical travel section. The traction that the locomotive can exert is mainly limited by the traction motor terminal voltage, the maximum current, and the adhesion conditions between the wheel and rail. If the traction motor is a DC motor, locomotive traction is also limited by the motor commutation. Therefore, in order to exert the limit capability of the electric traction locomotive, the motor has a maximum torque (current) limitation in the low speed zone; when the motor accelerates to a certain speed, it must be limited by the maximum power, ie, enter the constant power zone [21].

1.2.3 Classification of the AC Drive System

In order to study AC drive technology, many universities and research institutes have established their own AC drive test platforms based on actual conditions. Currently the popular AC drive test platform in the world can be divided into the following two categories:

1）Energy-consuming AC drive test platform

Energy-consuming AC drive test platforms are mainly divided into two types, as shown in Figure 1-1. The principle of the first type is relatively simple, that is, installing a resistance device with adjustable resistance torque on the output shaft of the test motor M, as shown in Figure 1-1 (a) [22]. By adjusting the magnitude of the resistive torque output by the resistance device, the effect of a simulated load can be achieved. This type of test platform

has the characteristics of simple structure and convenient operation, but there are also some deficiencies: ① The resistance torque resistance is set by adjusting the friction force between the test motor and the resistance device, and the resistance torque cannot be achieved with high precision; ② Kinetic energy output by the test motor is dissipated in the form of heat during the friction process, resulting in waste of energy, which is particularly prominent in high-power test platforms; ③ Resistance equipment can only simulate the static and slow changes of the load but it cannot simulate the dynamic change process of a real load in real time.

The second type of test platform has a wider range of applications than the first one, because it can simulate the dynamic process of actual load changes. The specific basic principle is: the test motor M is connected with a DC generator G, and the generator is connected with a resistive load R. The purpose of adjusting the resistance torque can be achieved by changing the size of the excitation L of the generator, thereby simulating the actual load, as shown in Figure 1-1(b) [22]. This type of test platform has a simple structure and is easy to control. However, the resistance R completely depletes the energy generated by the generator G, and the energy loss is too high, especially for a high-power AC drive test platform, which is costly. It is also necessary to consider how to dissipate the resistive load, which often increases the area of the equipment and the occupied laboratory. Therefore, the energy-consuming AC drive test platform is suitable for test platforms with low power and low performance requirements, and is not suitable for high-power test platforms.

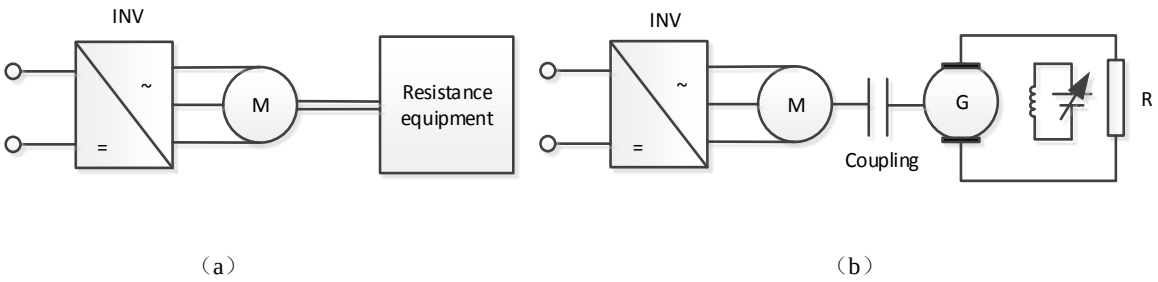

（a） （b）

Fig. 1-1 Energy-consuming AC drive test platform

2）Energy feedback AC drive test platform

The energy feedback AC drive test platform is mainly divided into the following three types: unit load feedback platform, grid-side energy multi-feedback test platform, and DC-side busbar energy multi-feed test platform [23].

The unit load feedback platform is a typical energy feedback test platform, which realizes the energy feedback by the unit load, as shown in Figure 1-2. The transformer supplies power to the converter. The converter provides three-phase alternating current for the asynchronous motor to drive the entire motor unit, and the synchronous generator generates electrical energy for feedback to the grid side. By adjusting the respective excitation parts of the "DC generator-DC motor-synchronous generator" unit, the output torque of the accompanying test motor can be changed, that is, the resistance torque of the test motor can be changed, and the frequency of the synchronous generator is maintained constant [24].

This kind of test platform can feed back part of the energy to the power grid during operation, save costs, and effectively improve energy utilization. However, this test platform also has some shortcomings: the entire test platform uses four motors, increasing the cost of the test platform; at the same time, the test platform needs to control four motors, which causes the control strategy to be very complicated. If the control method is improper, it will easily cause the entire system to fail. Finally, because the accompanying motor is a DC generator, the commutation problems of the DC motor cause that the accuracy and stability of the tester are not guaranteed when the test motor rotates at high speed.

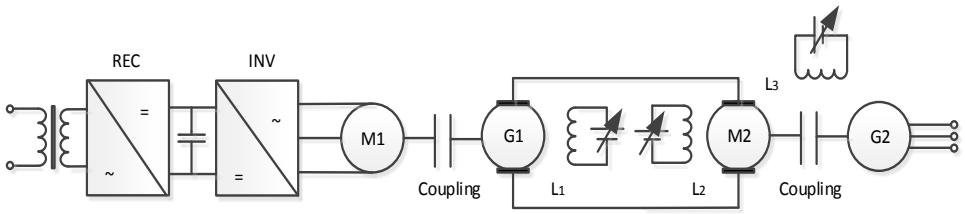

Fig. 1-2 Unit load feedback platform

The grid-side energy multi-feedback test platform consists of a four-quadrant operation converter and an asynchronous motor. The load motor generates electricity and the converter feeds back the energy sent to the grid, as shown in Figure 1-3. Compared with

other AC reciprocal test platforms, this type of test platform has obvious advantages in the following aspects: ①The test platform has a high energy utilization rate, and the energy loss is only the switching loss of the power electronic devices and the internal loss of the motor; ② The loss of the system only occupies a small part of the output power of the test motor. Therefore, this type of solution can be used to complete the test of a high-power motor with a smaller voltage level; ③ The test platform can meet the requirements for high-speed testing of traction motors: ④ System is symmetrical. The two groups of inverters have the same structure and function, and the two motors can be operated in the electric mode and the power generation mode, respectively. What's more, they can be both used as the measured motors, improving the work efficiency and reduces the workload [25]. However, the test platform requires that the power capacity of the system should be matched to the capacity of the test motor, and the test platform has high requirements on control strategy and power quality of the converter.

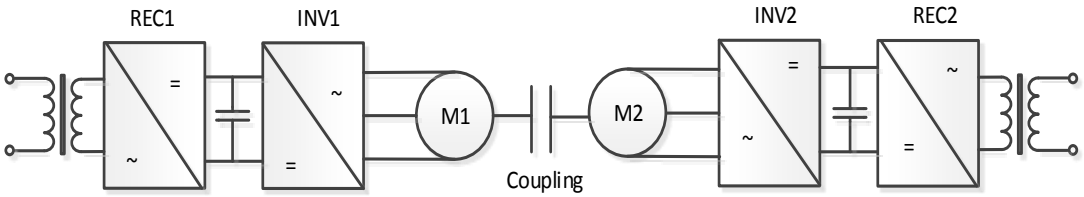

Fig. 1-3 Grid-side energy multi-feedback test platform

The DC-side busbar multi-feed test platform is composed of two identical inverters and a pair of coupled-axis asynchronous motors, where energy feedback occurs at the DC bus, as shown in Figure 1-4. The essence of the test platform is to convert the AC asynchronous motor into an alternator to simulate the load. At present, this type of DC-side busbar power multi-feed test platform is very popular in the world. This kind of test platform can also achieve the goal of saving energy and improving energy efficiency.

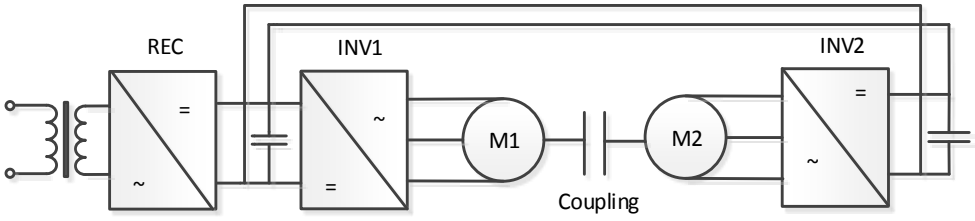

Fig. 1-4 DC-side busbar energy multi-feed test platform

1.3 Monitoring Device for Mutual Feedback AC Drive Test System

The mutual feedback AC drive test system is a complex multi-variable system that includes main circuit, control circuit, and upper computer. The control flow of the system is more complicated and if there is a problem in one link the entire system will easily fail or even go crash. The research of monitoring devices is of great significance to the entire rail transit industry. The monitoring device is a guarantee for the normal stable operation of a system. A complete monitoring device can significantly improve the stability and reliability of the AC drive system and reduce the maintenance cost. Therefore, a complete monitoring device is crucial for the mutual feedback AC drive test system. This article adopts CAN bus technology and RS485 serial port technology to develop the monitoring device.

The RS485 serial port technology adopts a half-duplex working mode and has the characteristics of balanced transmission and differential reception. Most of the two-wire systems use shielded twisted pairs for data communications. This two-wire connection method uses a bus topology model and can connect up to thirty-two nodes on a bus [26]. RS485 series port technology adopts the "master-slave" communication mode, that is, one host corresponds to multiple slaves at the same time. The RS485 serial communication technology has a low single point cost, but there are many obvious defects: low bus utilization, low data transmission efficiency, short communication distance, low communication success rate, and difficult network debugging.

Fieldbus is a serial, bidirection-transmission and multipoint-communication data bus installed between field devices and automatic control devices [27]. Fieldbus technology is mainly used to solve the problem of information communication, which provides a good complement to the disadvantages of the RS485 bus technology. The main types of fieldbuses are Profibus, LonWorks bus, Foundation Fieldbus and CAN bus. Fieldbus technology is a combination of computer networks and industrial automation technology, with good reliability, flexibility and system openness. Compared with the RS485 bus technology, the application of fieldbus technology has made significant improvements in the design, installation, operation and maintenance of monitoring devices.

CAN is an abbreviation of Controller Area Network and was developed by Bosch, a well-known automotive technology supplier in Germany. It is one of the most widely used fieldbuses in the world [28]. The stability and high performance of CAN bus technology have been recognized by the industry. The CAN bus protocol has become the standard protocol for the vehicle driving control unit and industrial automation in Europe and the United States, and it is also used in rail transit, chemical industry, aerospace, industrial automation, etc. Literature [29] proposes an AC drive monitoring system of urban rail based on CAN bus technology, which optimizes the urban rail transit layout.

1.4 Main works of This Paper

The designed low-power AC drive test platform is a simplified version of the high-power AC drive test platform, but it can realize all the functions of the high-power AC drive test platform. The final high-power mutual feedback AC drive test platform will be adopted in HXD_3 electric locomotives. The main work accomplished in this paper is as follows:

(1) The working principle and mathematical model of the single-phase PWM rectifier are studied. Three control strategies are adopted: PI control, proportional resonance control and repetitive control. The three control methods are simulated by Simulink simulation platform. The advantages and disadvantages of the three control strategies are analysed. Verification is carried out to verify the single-phase PWM rectifier based on repetitive control.

(2) The mathematical model and the vector control principle of the asynchronous motor are studied. A vector control system based on the rotor magnetic field orientation is established. The motor controller is designed and verified by simulation and experiment.

(3) The software and hardware design of the mutual feedback AC drive test system based on TMS320F28335DSP are completed. The construction of PWM rectifier and motor unit system are also completed. On this test platform, all tests for single-phase PWM rectifier, vector control system, and the function of energy feedback are all completed.

(4) According to the requirements of the mutual feedback AC drive test system, the establishment of the monitoring device is completed based on the CAN bus technology and the RS485 serial port technology, including the setting of the communication flow, the programming of each submodule, and the software and hardware debugging.

2 RESEARCH ON SINGLE-PHASE PWM RECTIFIER

The low-power AC test platform is a simplified version of the high-power AC drive test platform, but it can realize a complete test function of accurately simulating the operating characteristics of the electric locomotive and verifying that two low-power traction converters drive two coaxial low-power three-phase asynchronous motor respectively. Besides, the system can realize the function of energy feedback. The physical picture of the system is shown in Fig.2-1. This chapter mainly focuses on the research of single-phase PWM rectifier.

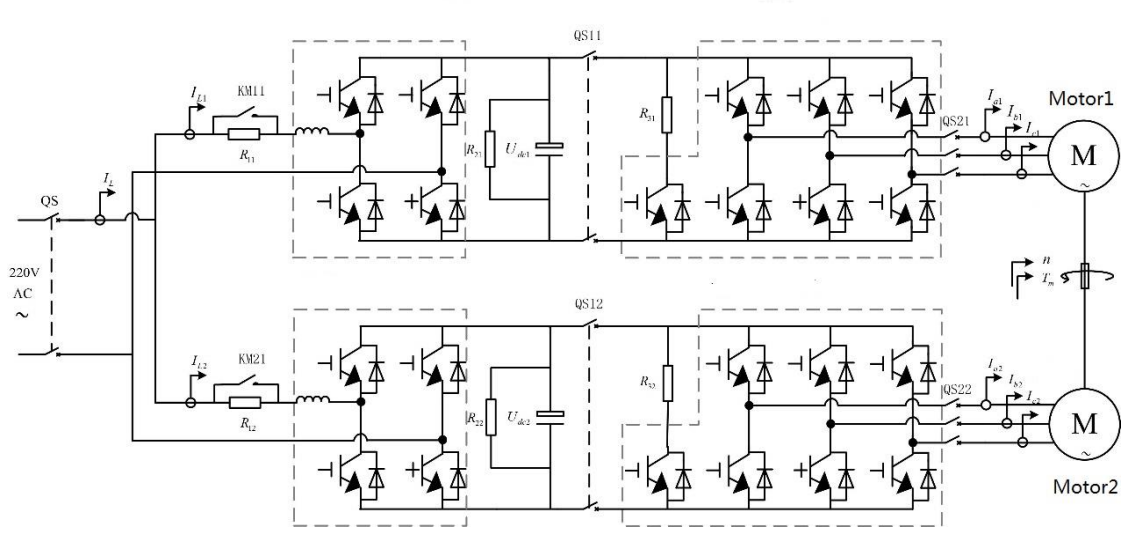

Fig. 2-1 Topology of the mutual feedback AC drive test system

2.1 Working Principle of Single-phase PWM Rectifier

Single-phase PWM rectifiers have a variety of topologies. This paper adopts a full-bridge single-phase PWM rectifier. Figure 2-2 shows the topology of the full-bridge single-phase PWM rectifier. According to Figure 2-2, it consists of four power switching devices and

only one capacitor which is used as the energy storage capacitor on the DC side, which is easy to control.

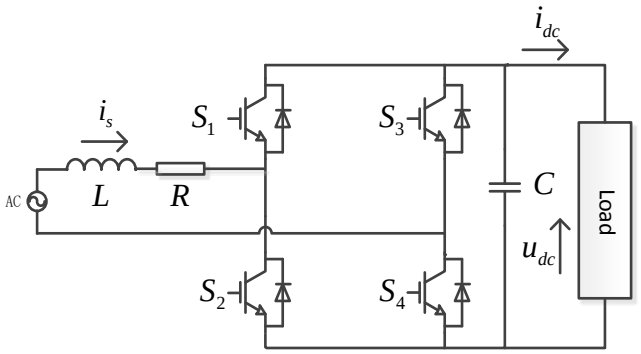

Fig. 2-2 Topology of the full-bridge single-phase PWM rectifier

The general PWM rectifier has two realization goals: On the one hand, the input power factor is required to be 1. On the other hand, the stability of the DC bus voltage must be maintained.

When the single-phase PWM rectifier sub-system is operated in a steady state, it can realize four-quadrant operation of the converter. The AC steady state characteristics of four typical full-bridge single-phase PWM rectifiers are selected here, as shown in Figure 2-3. From Figure 2-3 it can be seen that for the entire mutual feedback AC drive test platform, when the converter unit is in the electric state, the corresponding single-phase PWM rectifier is in the positive resistance characteristic zone, and the rectifier absorbs energy from the grid side. Correspondingly, when the converter unit is operating in the power generation state, the corresponding single-phase PWM rectifier is in the negative resistance characteristic zone. At this point, the rectifier transmits energy to the grid side.

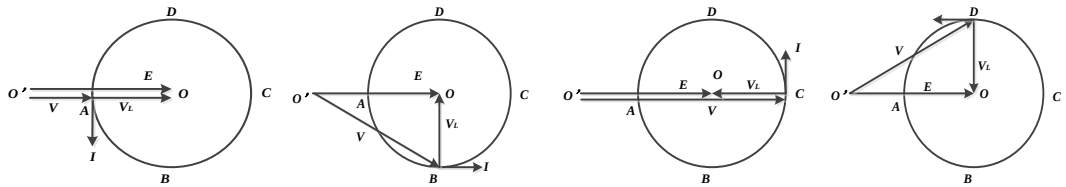

(a) Pure inductance characteristics (b) Positive resistance characteristics (c) Pure capacitance characteristics (d) Negative resistance characteristics

Fig. 2-3 AC side steady-state vector relationship of the full-bridge single-phase PWM rectifier

2.2 Mathematical Model of Single-phase PWM Rectifier

The simplified topology of the full-bridge single-phase PWM rectifier is shown in Figure 2-4.

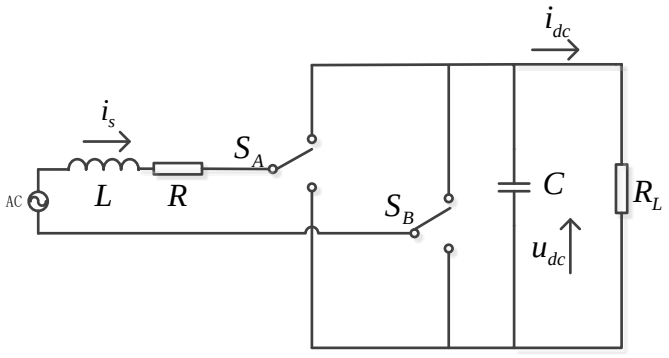

Fig. 2-4 Simplified topology of the full-bridge single-phase PWM rectifier

In order to simplify the process of the establishment of the mathematical model, the power electronic switch in Figure 2-2 is regarded as an ideal device. The state equation of its switching function is shown in the following equation.

$$S_A = \begin{cases} 1 & S_1 \text{ on}, S_2 \text{ off} \\ 0 & S_1 \text{ off}, S_2 \text{ on} \end{cases} \tag{2-1}$$

$$S_B = \begin{cases} 1 & S_3 \text{ on}, S_4 \text{ off} \\ 0 & S_3 \text{ off}, S_4 \text{ on} \end{cases} \tag{2-2}$$

Because the upper and lower bridges of a full-bridge circuit are turned on in turn, two switching devices will produce four combinations. The voltage on the AC side of the rectifier has three values:

$$u_{ab} = \begin{cases} u_{dc} & S_A{=}1, S_B = 0 \\ 0 & S_A{=}0, S_B = 0 \text{ or } S_A{=}1, S_B = 1 \\ -u_{dc} & S_A{=}0, S_B = 1 \end{cases} \tag{2-3}$$

The relationship between the voltage on the AC side of the rectifier bridge and the switching function is:

$$u_{ab} = (S_A - S_B)u_{\mathrm{dc}} \tag{2-4}$$

The AC side circuit of the single-phase PWM rectifier is simplified, as shown in Figure 2-5.

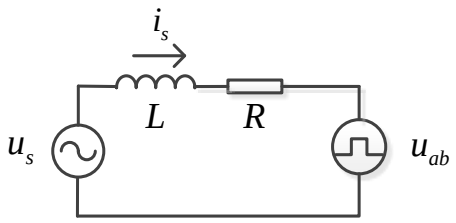

Fig. 2-5 Simplified circuit of the AC side of the single-phase PWM rectifier

According to Figure 2-5, the voltage vector balance equation of the AC side of the single-phase PWM rectifier can be obtained:

$$u_s = u_{ab} + Ri_s + L\frac{di_s}{dt} \tag{2-5}$$

Assuming that the power switching devices in the figure are all ideal components, there is no energy loss in the device itself. According to the law of conservation of energy, the instantaneous power at the AC and DC sides of the rectifier is equal, ie:

$$u_s i_s = u_{dc} i_0 \tag{2-6}$$

From Figure 2-4, it can be seen that:

$$i_0 = (S_A - S_B)\mathrm{i}_s \tag{2-7}$$

The current balance equation on the DC side of the single-phase PWM rectifier can be obtained from Kirchhoff's current law (KCL):

$$i_0 = \frac{u_{dc}}{R_L} + C\frac{\mathrm{d}u_{dc}}{dt} \tag{2-8}$$

According to the Equations (2-4), (2-5), (2-7), and (2-8), the state equation of the single-phase PWM rectifier can be obtained as:

$$\begin{cases} L\dfrac{di_s}{dt} = u_s - i_s R - (\mathrm{S}_A - \mathrm{S}_B)\,\mathrm{u}_{dc} \\ C\dfrac{du_{dc}}{dt} = (\mathrm{S}_A - \mathrm{S}_B)\,\mathrm{i}_s - \dfrac{u_{dc}}{R_L} \end{cases} \tag{2-9}$$

According to Equation (2-9), based on the desired control target, an appropriate control strategy can be selected to control the input current and the DC voltage of the rectifier.

2.3 Control Strategy of Single-phase PWM Rectifier

For the control of single-phase PWM converter, on the one hand it requires the stable DC voltage; on the other hand it requires the AC side can achieve unity power factor operation while ensuring that the harmonic of the AC input current is suppressed. The two goals are both closely related to the input current, so the input current control is the key to single-phase PWM rectifier control. In order to improve the dynamic response performance and reduce the dependence of control performance on main circuit parameters, this paper adopts direct current control method.

2.3.1 PI Control

For the single-phase PWM rectifier, the traditional PI control cannot suppress the interference of the grid-side voltage to the system. This paper adds a voltage feed-forward link to the traditional PI control strategy and enhances the dynamic performance of the system [30]. The specific control block diagram is shown in Figure 2-6. The control strategy uses double closed-loop control of the voltage outer loop and the current inner loop [31]. The outer loop is a DC voltage loop, and a PI controller is used to adjust the DC side voltage to obtain the stable DC side bus voltage; the product of the output of the voltage outer loop and the phase angle obtained by the voltage phase locked loop (PLL) is the reference value of the current inner loop. The AC input current is controlled by the P controller so as to achieve the control target. Finally, the normal operation of the single-phase PWM rectifier can be achieved through the SPWM algorithm.

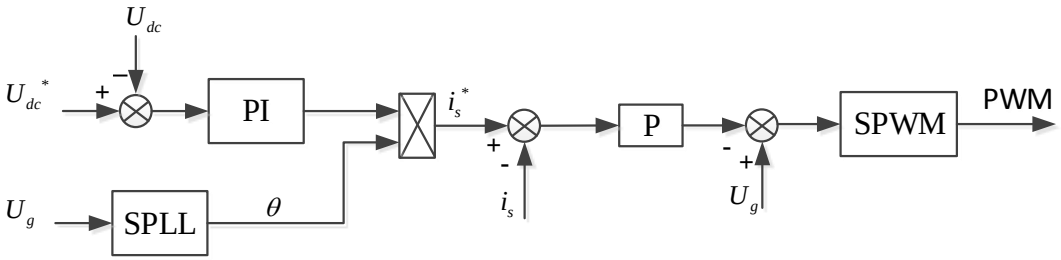

Fig. 2-6 Control block diagram of feed-forward PI

Considering the delay caused by the data sampling and the inertia of the PWM rectifier, according to the control block diagram of Figure 2-6, the control block diagram of the input current loop of the AC side can be obtained, as shown in Figure 2-7.

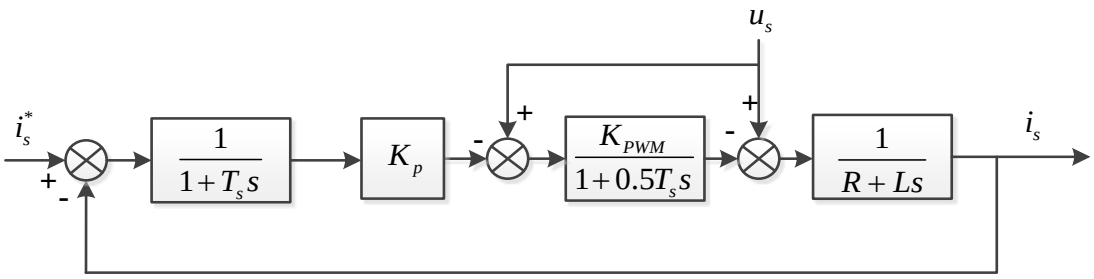

Fig. 2-7 Control block diagram of the input current loop of the AC side

Among them, T_s is the AC input current sampling cycle but also the PWM switching cycle; K_P is the control parameter of P controller; K_{PWM} is the equivalent gain of the single-phase PWM rectifier; $\boldsymbol{i}_s^*$ is the reference value of the input current; u_s is the voltage disturbance. In order to select the appropriate parameter of the P controller, to obtain the desired control effect, the control block diagram in Figure 2-7 is simplified, in which the two inertial quantities are combined and the interference amount is ignored. The simplified control block diagram of the input current loop of the AC side is shown in Figure 2-8.

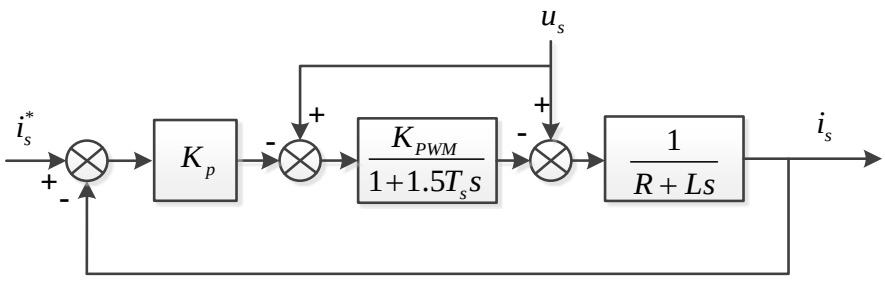

Fig. 2-8 Simplified control block diagram of the input current loop of the AC side

According to Figure 2-8, it can be seen that the open-loop transfer function of this system is:

$$G(s)=\frac{K_P}{(1.5T_s s)(\mathrm{R}+Ls)} \qquad (2\text{-}10)$$

Considering the ideal condition, the resistance R of the rectifier can be neglected. The closed-loop transfer function of the inner current loop can be obtained by the Equation (2-10):

$$G_c(s)=\frac{G(s)}{1+G(s)}=\frac{K_P}{1.5LT_s s^2+Ls+K_P} \tag{2-11}$$

In the formula： $T_s=\frac{1}{150000}s$； $L=4mH$.

According to the order of the closed-loop transfer function of the system, the current loop is set as a typical type I system. However, from Equation (2-11), the transfer function is not a standard form of a typical type I system, and Equation (2-11) can be simplified in this form:

$$G_c(s)\approx\frac{K_P}{1.5LT_s s^2+Ls}=\frac{K_P}{s(1.5LT_s s+L)} \tag{2-12}$$

Let $K_p=20$， then the inner current loop is corrected to be a typical type I system. Figure 2-9 is the Bode diagram of the open loop transfer function of the current inner loop.

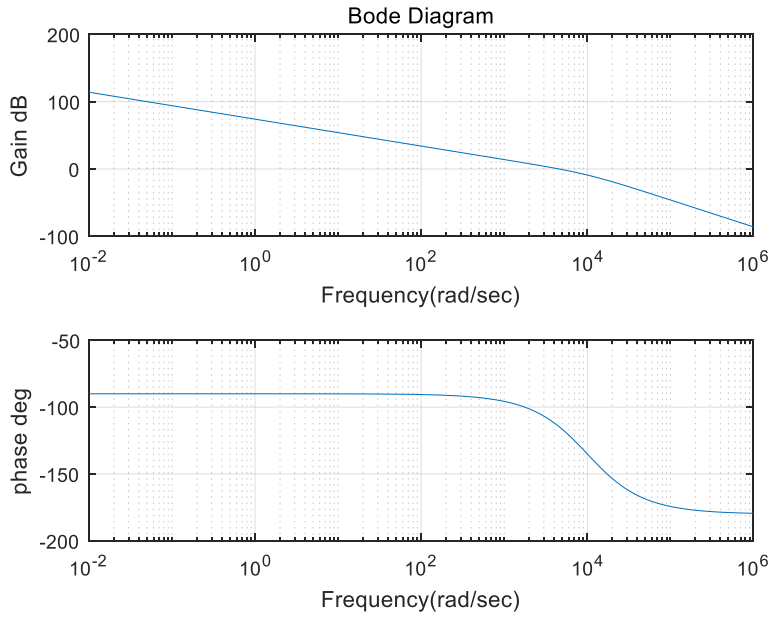

Fig. 2-9 Bode diagram of the open loop transfer function of the current inner loop

Because in the voltage outer loop controller, the output of the DC voltage outer loop determines the current reference value of the inner current loop, but the entire control loop has time-varying links, so the design of the outer loop of the voltage brings some difficulty. Because the current loop has a certain bandwidth, the current loop can be regarded as a proportional loop where the gain of the closed loop transfer function of the inner loop is

gained at the fundamental frequency. At this point the control block diagram of voltage outer loop controller can be equivalent to Figure 2-10.

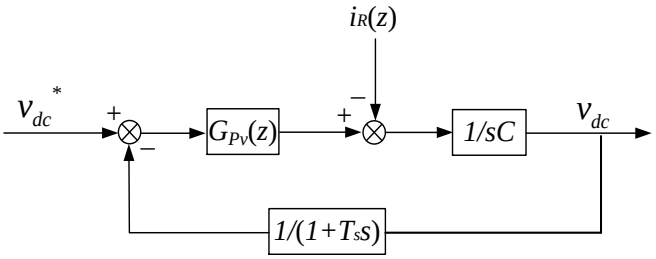

Fig. 2-10 Control block diagram of voltage outer loop controller

It can be seen that its open-loop transfer function is:

$$G_{ov}(s) = G_{pv}(s)H(s) = \frac{1}{C}\frac{k_{pv}s + k_{iv}}{s^2(T_s s + 1)} \tag{2-13}$$

Because the DC-side voltage of the single-phase PWM rectifier has instantaneous secondary ripple, in order to prevent the secondary ripple from affecting the given value of the current inner loop, the parameters of the PI controller are selected so that the open-loop transfer function crossover frequency is 10 Hz.

According to the above design principles, it is necessary to make:

$$\begin{cases} \left| \frac{1}{C}\frac{k_{pv}s + k_{iv}}{s^2(Ts+1)} \right|_{s=j2\pi f_{wc}=j20\pi} = 1 \\ \frac{k_{iv}}{k_{pv}} = 2\pi f_{wz} = 20 \end{cases} \tag{2-14}$$

Therefore, the parameters of the voltage outer loop controller can be obtained. k_{pv} is equal to 0.5 and k_{iv} is equal to 10. At this point the Bode diagram of the open loop transfer function of the voltage outer loop is shown in Figure 2-11.

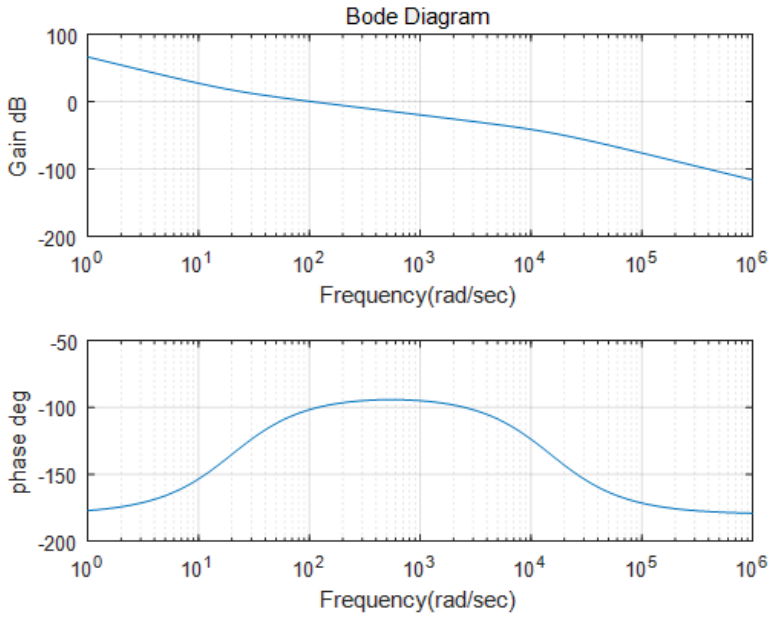

Fig. 2-11 Bode diagram of the open loop transfer function of the voltage outer loop

2.3.2 Proportional Resonance Control

PI control has good robustness and rapidity, but it cannot achieve no difference adjustment for the control of AC value. In this section, a proportional resonance controller is used to realize the no-difference adjustment of the AC variable, eliminating the steady-state error, and simultaneously suppressing the harmonics of AC side. The basic principle of proportional resonance control is to introduce near-infinity gain at the fundamental frequency of the sine wave to eliminate the steady-state error [32].

The ideal transfer function of a proportional resonant controller is:

$$G(s) = K_P + \frac{2K_R s}{s^2 + w^2} \qquad (2\text{-}15)$$

In the formula， K_P is the proportional coefficient， K_R is the resonance coefficient and w is the resonance angle frequency. Assuming K_P = 0.5, K_R =100 and w =314rad/s, the Bode diagram of the ideal transfer function of the proportional resonant controller is shown in Figure 2-12. It can be seen that the system has a near-infinity gain at the resonant frequency.

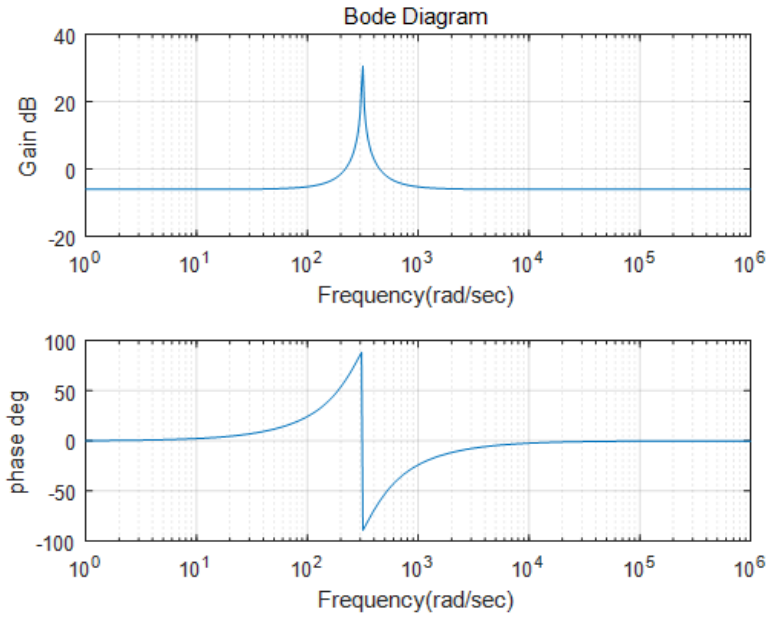

Fig. 2-12 Bode diagram of the ideal transfer function of the proportional resonant controller

With reference to Figure 2-8 and Equation (2-15), the control block diagram of input current loop using the proportional resonant controller can be obtained, as shown in Figure 2-13.

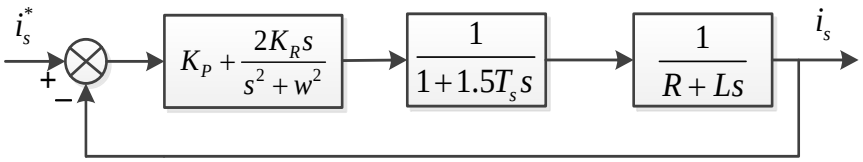

Fig. 2-13 Control block diagram of input current loop using the proportional resonant controller

According to Fig.2-13, the resistance of the rectifier can be neglected under ideal conditions. At this point, the closed-loop transfer function of the current loop is:

$$G_c(s) = \frac{G(s)}{1+G(s)} = \frac{K_P s^2 + 2K_R s + K_P w^2}{1.5LT_s s^4 + (K_P + 1.5LT_s)s^2 + 2K_R s + K_P w^2} \quad (2\text{-}16)$$

In an actual project, infinite gain is unachievable and excessive gain can destabilize the system. Especially at the resonant frequency, the ideal gain of the proportional resonant controller will affect the power regulation of the power grid. Therefore, in the actual project, a modified proportional resonance controller is often applied [33] . Its transfer function is:

$$G(s) = K_P + \frac{2K_R w_c s}{s^2 + 2w_c s + w^2} \quad (2\text{-}17)$$

In the formula， K_P is the proportional coefficient， K_R is the resonance coefficient， w_c is the cut-off frequency and w is the resonance angle frequency. Assuming K_P = 0.5, K_R =100, w_c =10rad/s and w =314rad/s, the Bode diagram of the transfer function of the modified proportional resonant controller is shown in Figure 2-14. According to Figure 2-14, the gain at the resonant frequency is 40dB, which is enough to eliminate the steady-state error of the system. At the same time, the width of the resonant frequency bandwidth increases, and the anti-interference ability of the system increases.

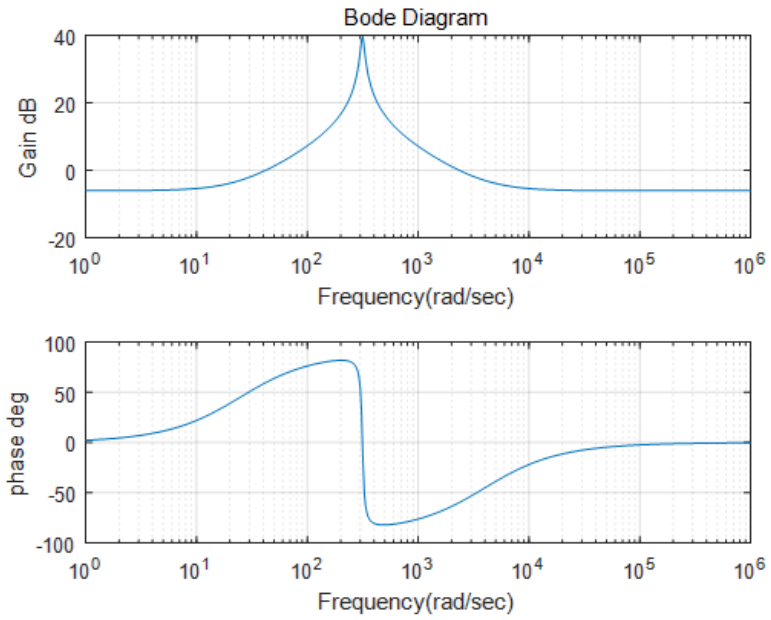

Fig. 2-14 Bode diagram of the transfer function of the modified proportional resonant controller

2.3.3 Repetitive Control

Repetitive control has better results in eliminating steady-state errors and improving steady-state performance. At the same time, it can effectively improve power quality and suppress grid interference. Therefore, this paper introduces repetitive control on the basis of traditional proportional control, which not only ensures the system has a faster response speed, but also has a good steady-state compensation effect. Figure 2-15 is the block diagram of the embedded repetitive controller applied in this paper.

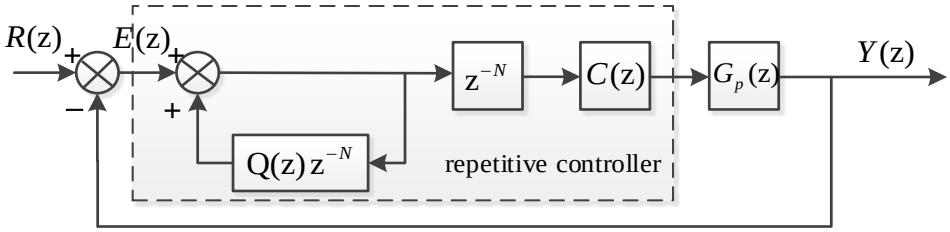

Fig. 2-15 Block diagram of the embedded repetitive controller

The feedback element $Q(z)z^{-N}$ does not accumulate all the errors of the previous cycle, but only accumulates some of them. Although this will make the steady-state error of the system non-zero, it can change the open-loop pole position of the system and improve the stability, which can essentially be considered as sacrificing the steady-state accuracy of the system in exchange for system stability. $Q(z)$ is usually chosen as an integer less than 1 or as a low-pass filter.

The periodic delay element z^{-N} serves as an important part of implementing the advance compensation, so that the error of this cycle has an effect in the next cycle, that is, a delay of one cycle leads to an advancement. The compensator $C(z)$ designed for the control object provides amplitude and phase compensation for the control object $G_p(z)$.

It can be concluded that the transfer function of the error signal for the reference signal is:

$$\frac{E(z)}{R(z)}=\frac{1-Q(z)z^{-N}}{1-[Q(z)-C(z)G_p(z)]z^{-N}} \tag{2-18}$$

According to Equation (2-18), a sufficient condition for system stability can be obtained by combining the small gain principle [34]:

$$\left|Q(e^{j\omega T})-C(e^{j\omega T})G_p(e^{j\omega T})\right|<1 \qquad \omega\in[0,\pi/T]$$

Where T is the sampling period, sampling is performed at the switching frequency in this paper, that is, $T=T_D=T_s=1/15000$s.

From the above sufficient conditions, it can be seen that as long as $|Q(z)\text{-}C(z)G_p(z)|$ is less than 1 in the entire frequency band, the system can be judged to be stable. To fully compensate the controlled object, ie, $C(z)=G_p(z)^{-1}$. $Q(z)$ must be set to 1 to satisfy the stability of the whole frequency band. But $Q(z)$ is usually selected as an integer less than 1, and it can be analyzed that in this case the system will not be able to satisfy the full-band stability. However, in the actual current compensation control carried out in this paper, the

controlled object mainly exists in the low-middle frequency band, so as long as $C(z)G_p(z)$ satisfies zero-phase shift with unity gain in the low-middle frequency band and has high-frequency fastness attenuation, the system can be judged to be stable [35].

In the specific design process of repetitive controller, since the controlled object is usually more complex, and the delay under digital control further strengthens its complexity, it is generally first to consider the control characteristics of each step in the repetitive controller. And then it necessary to verify the stability of the entire system according to related stability criteria. The following describes the design method of each link.

According to Figure 2-15, it can be seen that the repetitive signal generator is:

$$G_{rep}(z)=\frac{1}{1-Q(z)z^{-N}} \tag{2-19}$$

In this paper, $Q(z)$ is selected to 0.95 in the current compensation design, and Figure 2-16 is the Bode diagram of the repetitive signal generator when $Q(z)$ is equal to 0.95. From Fig.2-16, it can be seen that the fundamental gain of $G_{rep}(z)$ and the gain of each harmonic are relatively large, and the phase is always between -90° and +90°, meeting the requirements of harmonic compensation.

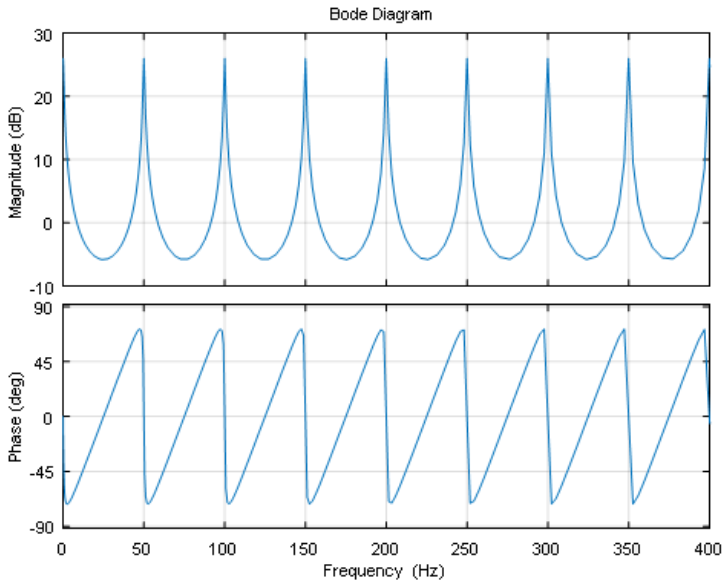

Fig. 2-16 Bode diagram of the repetitive signal generator

The compensator $C(z)$ has the following expression:

$$C(z) = k_r \cdot z^k \cdot S(z) \tag{2-20}$$

Among them, k_r is the gain coefficient, that is to realize the amplitude compensation; z^k is the advance compensation link, that is to carry on the phase compensation; $S(z)$ is the filter, which corrects the gain of the middle and low frequency band, restrains the resonance peak of the controlled system and improves the high-frequency attenuation characteristics of the system.

The gain coefficient k_r is usually a value not greater than 1. Larger k_r provides larger amplitude compensation to make the system obtain faster convergence speed, but at the same time it will reduce the stability of the system; On the contrary, a smaller k_r will reduce the convergence speed and enhance the stability of the system. Considering that there is also instruction feedforward for amplitude compensation in this paper, k_r is set to 0.5.

Therefore, a second-order low-pass filter is designed as $S(z)$, which is mainly used to provide high-frequency attenuation characteristics for the system. Considering that current compensation requires a certain bandwidth for harmonic compensation, so a second-order low-pass filter with cut-off frequency of 1000 Hz and damping coefficient of 0.707 is selected in this paper:

$$S(z) = \frac{0.0327z^2 + 0.0655z + 0.0327}{z^2 - 1.427z + 0.558} \tag{2-21}$$

The advanced compensation link z^k is used to offset the phase lag of the $S(z)G_p(z)$ in the middle and low frequency bands. In combination with the design $S(z)$, the system control object, and the delay caused by the actual digital control, k is set to 5.

So the expression of compensator C(z) is:

$$C(z) = 0.5z^5 \frac{0.0327z^2 + 0.0655z + 0.0327}{z^2 - 1.427z + 0.558} \tag{2-22}$$

At this point, the expression of the repetitive controller is:

$$H_{rep}(z) = \frac{0.5z^{-295}}{1 - 0.95z^{-300}} \frac{0.0327z^2 + 0.0655z + 0.0327}{z^2 - 1.427z + 0.558} \tag{2-23}$$

According to Equation (2-23), the Bode diagram of the final repetitive controller is shown in Figure 2-17. It is not difficult to find that there is a large gain at the fundamental wave and each harmonic, which can effectively compensate the harmonic current.

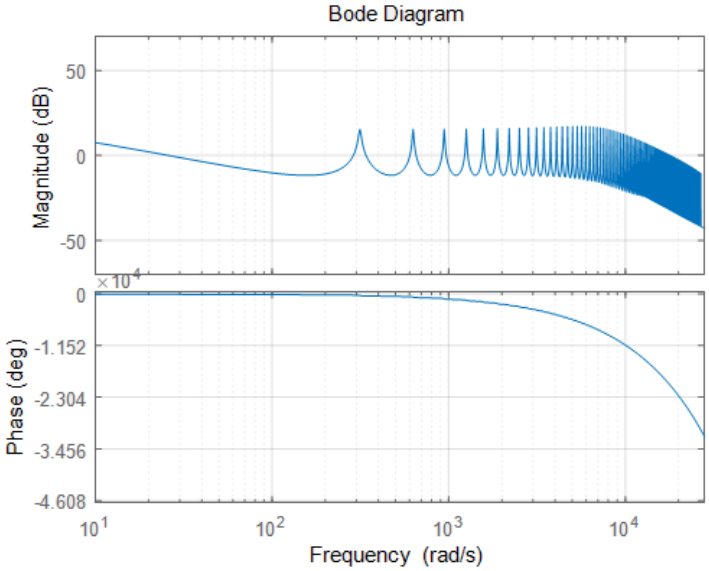

Fig. 2-17 Bode diagram of the repetitive controller

According to Figure 2-7, it can be seen that the control object of the repetitive controller is:

$$G_p(s)=\frac{(1+1.5T_s\,\mathrm{s})Ls}{(1+1.5T_s\,\mathrm{s})Ls+1} \tag{2-24}$$

By applying bilinear transformation to $G_p(s)$, the Nyquist plot of $H_{rep}(z)G_p(z)$ can be obtained, as shown in Figure 2-18.

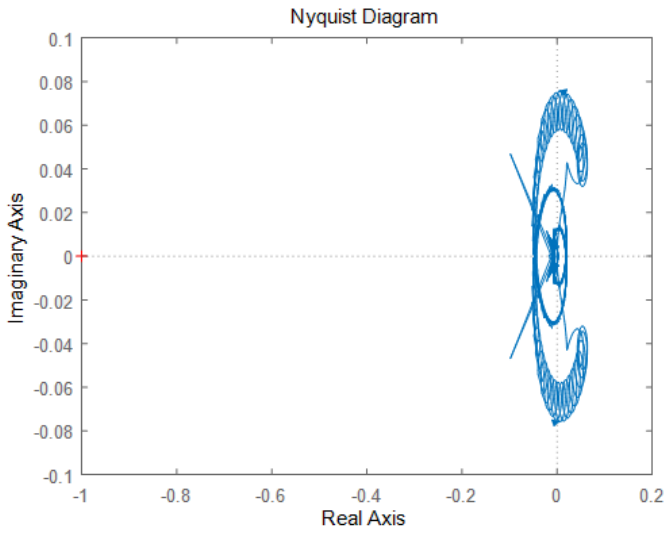

Fig. 2-18 Nyquist plot of $H_{rep}(z)G_p(z)$

It can be seen that the trajectory does not include the point(-1, j0), so the system can be considered stable at this point.

2.4 Summary

This chapter first introduces the working principle and mathematical model of the single-phase PWM rectifier; then according to its mathematical model, PI controller, proportional resonance control and repetitive control are used to design the controller. Finally, the stability of the controller is verified.

3 RESEARCH ON VECTOR CONTROL SYSTEM BASED ON ROTOR MAGNETIC FIELD ORIENTATION

Compared with the traditional DC motor, the speed regulation system of the asynchronous motor is more complicated. Because asynchronous motor is a high-order, nonlinear, strongly coupled multivariable system [36]. By the coordinate transformation, the decoupling of the flux linkage and the rotation speed of the asynchronous motor can be realized, and the dynamic and static characteristics can reach the level which is comparable to the DC motor. This chapter firstly introduces the mathematical model of the asynchronous motor, and then introduces the principle of vector control system based on rotor magnetic field orientation. Finally, the controllers of the vector control system are designed, and the stability of the controllers verified.

3.1 Mathematical Model of Asynchronous Motor

3.1.1 Mathematical Model of Asynchronous Motor in Three-phase Static Coordinate System

Figure 3-1 is the T-type equivalent circuit of the asynchronous motor in the three-phase stationary coordinate system. Among them, u_X、i_X、ψ_X represent the stator voltage, stator current and flux linkage of a certain phase respectively and u_x、i_x、ψ_x represent the rotor voltage, rotor current and flux linkage of the phase. According to the equivalent circuit, the voltage equation, flux linkage equation and torque equation of the asynchronous motor in the three-phase stationary coordinate system can be derived.

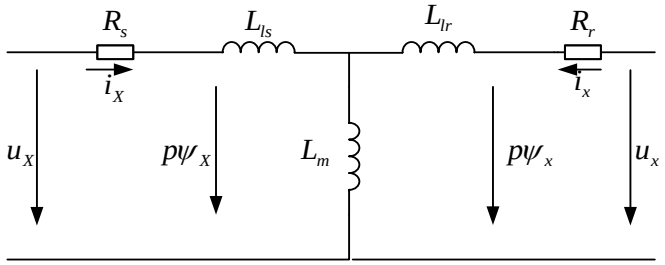

Fig. 3-1 T-type equivalent circuit of the asynchronous motor in the three-phase coordinate system

$$\begin{bmatrix} u_{\mathrm{A}} \\ u_{\mathrm{B}} \\ u_{\mathrm{C}} \\ u_{\mathrm{a}} \\ u_{\mathrm{b}} \\ u_{\mathrm{c}} \end{bmatrix} = \begin{bmatrix} R_{\mathrm{s}} & 0 & 0 & 0 & 0 & 0 \\ 0 & R_{\mathrm{s}} & 0 & 0 & 0 & 0 \\ 0 & 0 & R_{\mathrm{s}} & 0 & 0 & 0 \\ 0 & 0 & 0 & R_{\mathrm{r}} & 0 & 0 \\ 0 & 0 & 0 & 0 & R_{\mathrm{r}} & 0 \\ 0 & 0 & 0 & 0 & 0 & R_{\mathrm{r}} \end{bmatrix} \begin{bmatrix} i_{\mathrm{A}} \\ i_{\mathrm{B}} \\ i_{\mathrm{C}} \\ i_{\mathrm{a}} \\ i_{\mathrm{b}} \\ i_{\mathrm{c}} \end{bmatrix} + p \begin{bmatrix} \psi_{\mathrm{A}} \\ \psi_{\mathrm{B}} \\ \psi_{\mathrm{C}} \\ \psi_{\mathrm{a}} \\ \psi_{\mathrm{b}} \\ \psi_{\mathrm{c}} \end{bmatrix} \tag{3-1}$$

$$\begin{bmatrix} \psi_{\mathrm{A}} \\ \psi_{\mathrm{B}} \\ \psi_{\mathrm{C}} \\ \psi_{\mathrm{a}} \\ \psi_{\mathrm{b}} \\ \psi_{\mathrm{c}} \end{bmatrix} = \begin{bmatrix} L_{\mathrm{AA}} & L_{\mathrm{AB}} & L_{\mathrm{AC}} & L_{\mathrm{Aa}} & L_{\mathrm{Ab}} & L_{\mathrm{Ac}} \\ L_{\mathrm{BA}} & L_{\mathrm{BB}} & L_{\mathrm{BC}} & L_{\mathrm{Ba}} & L_{\mathrm{Bb}} & L_{\mathrm{Bc}} \\ L_{\mathrm{CA}} & L_{\mathrm{CB}} & L_{\mathrm{CC}} & L_{\mathrm{Ca}} & L_{\mathrm{Cb}} & L_{\mathrm{Cc}} \\ L_{\mathrm{aA}} & L_{\mathrm{aB}} & L_{\mathrm{aC}} & L_{\mathrm{aa}} & L_{\mathrm{ab}} & L_{\mathrm{ac}} \\ L_{\mathrm{bA}} & L_{\mathrm{bB}} & L_{\mathrm{bC}} & L_{\mathrm{ba}} & L_{\mathrm{bb}} & L_{\mathrm{bc}} \\ L_{\mathrm{cA}} & L_{\mathrm{cB}} & L_{\mathrm{cC}} & L_{\mathrm{ca}} & L_{\mathrm{cb}} & L_{\mathrm{cC}} \end{bmatrix} \begin{bmatrix} i_{\mathrm{A}} \\ i_{\mathrm{B}} \\ i_{\mathrm{C}} \\ i_{\mathrm{a}} \\ i_{\mathrm{b}} \\ i_{\mathrm{c}} \end{bmatrix} \tag{3-2}$$

$$\begin{aligned} \mathrm{T}_e = n_p[&(i_{\mathrm{A}}i_{\mathrm{a}} + i_{\mathrm{B}}i_{\mathrm{b}} + i_{\mathrm{C}}i_{\mathrm{c}})\sin\theta + (i_{\mathrm{A}}i_{\mathrm{b}} + i_{\mathrm{B}}i_{\mathrm{c}} + i_{\mathrm{C}}i_{\mathrm{a}})\sin(\theta + 120^o) \\ &+ (i_{\mathrm{A}}i_{\mathrm{b}} + i_{\mathrm{B}}i_{\mathrm{c}} + i_{\mathrm{C}}i_{\mathrm{a}})\sin(\theta - 120^o)] \end{aligned} \tag{3-3}$$

According to the Equations (3-1), (3-2) and (3-3), it can be seen that in the asynchronous motor, the coupling among the voltage, current, speed, torque and other parameters exists. It is not conducive to the design of control system, so it is necessary to simplify it in the two-phase rotating coordinate system.

3.1.2 Mathematical Model of Asynchronous Motor in Two-phase Rotating Coordinate System

Fig. 3-2 is the T-type equivalent circuit of the asynchronous motor in two-phase rotating coordinate system after coordinate transformation. w_{dqs} is the angular velocity of the dq rotating coordinate system relative to the rotor of the motor.

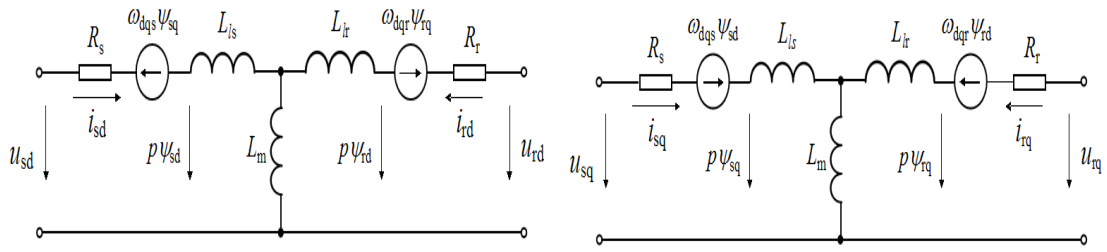

a. D-axis equivalent circuit b. Q-axis equivalent circuit

Fig. 3-2 T-type equivalent circuit of the asynchronous motor in the two-phase rotating coordinate system

According to the equivalent circuit, the voltage equation, flux linkage equation and torque equation of the asynchronous motor in the two-phase rotating coordinate system can be derived：

$$\begin{cases} u_{sd} = R_s i_{sd} + p\psi_{sd} - \omega_{dqs}\psi_{sq} \\ u_{sq} = R_s i_{sq} + p\psi_{sq} + \omega_{dqs}\psi_{sd} \\ u_{rd} = R_r i_{rd} + p\psi_{rd} - \omega_{dqr}\psi_{rq} \\ u_{rq} = R_r i_{rq} + p\psi_{rq} + \omega_{dqr}\psi_{rd} \end{cases} \tag{3-4}$$

$$\begin{cases} \psi_{sd} = L_s i_{sd} + L_m i_{rd} \\ \psi_{sq} = L_s i_{sq} + L_m i_{rq} \\ \psi_{rd} = L_m i_{sd} + L_r i_{rd} \\ \psi_{rq} = L_m i_{sq} + L_r i_{rq} \end{cases} \tag{3-5}$$

$$T_{em} = n_p L_m (i_{sq}\psi_{sd} - i_{sd}\psi_{sq}) / L_r \tag{3-6}$$

According to the Equations (3-4), (3-5), and (3-6), it can be seen that although the order of the system is simplified, the problem of coupling between the parameters is still not completely resolved, so the next step is to do the rotor magnetic field orientation on it.

3.2 Vector Control Theory Based on Rotor Magnetic Field Orientation

In the vector control system based on rotor magnetic field orientation, when the d-axis in the dq coordinate system is oriented in the direction of the rotor flux linkage, the flux linkage component on the q-axis perpendicular to the d-axis is zero. Considering the internal short circuit of the rotor of the squirrel-cage asynchronous motor, the voltage equation and the flux linkage equation of the asynchronous motor can be expressed as:

$$\begin{cases} u_{sd} = R_s i_{sd} + p\psi_{sd} - \omega_s \psi_{sq} \\ u_{sq} = R_s i_{sq} + p\psi_{sq} + \omega_s \psi_{sd} \\ 0 = R_r i_{rd} + p\psi_{rd} \\ 0 = R_r i_{rq} + \omega_{sl} \psi_{rd} \end{cases} \quad (3\text{-}7)$$

$$\begin{cases} \psi_{sd} = L_s i_{sd} + L_m i_{rd} \\ \psi_{sq} = L_s i_{sq} + L_m i_{rq} \\ \psi_{rd} = L_m i_{sd} + L_r i_{rd} \\ 0 = L_m i_{sq} + L_r i_{rq} \end{cases} \quad (3\text{-}8)$$

Because the method adopted in this paper is based on rotor field orientation, the stator flux component in Equation (3-8) needs to be eliminated. Substituting Equation (3-8) into Equation (3-7) yields:

$$u_{sd} = R_s i_{sd} + p(L_s i_{sd} + L_m i_{rd}) - \omega_s (L_s i_{sq} + L_m i_{rq}) \quad (3\text{-}9)$$

$$u_{sq} = R_s i_{sq} + p(L_s i_{sq} + L_m i_{rq}) + \omega_s (L_s i_{sd} + L_m i_{rd}) \quad (3\text{-}10)$$

Because the rotor current cannot be measured, the rotor current component needs to be eliminated. The following equations can be obtained from Equation (3-8) :

$$i_{rq} = -\frac{L_m}{L_r} i_{sq} \quad (3\text{-}11)$$

$$i_{rd} = \frac{\psi_{rd} - L_m i_{sd}}{L_r} \quad (3\text{-}12)$$

Substituting Equations (3-11) and (3-12) into Equations (3-9) and (3-10) yields：

$$u_{sd} = R_s i_{sd} + \sigma L_s p i_{sd} + \frac{p L_m^{\ 2}}{L_r + L_r \tau_r p} i_{sd} - \omega_s \sigma L_s i_{sq} \quad (3\text{-}13)$$

$$u_{sq} = R_s i_{sq} + \sigma L_s p i_{sq} + \omega_s (\sigma L_s i_{sd} + \frac{L_m}{L_r} \psi_{rd}) \quad (3\text{-}14)$$

Equations (3-13) and (3-14) are the voltage equations of the vector control system based on rotor magnetic field orientation. The flux linkage equation, slip equation and torque equation of the motor can also be obtained:

$$\psi_{\mathrm{rd}} = \frac{L_{\mathrm{m}}}{1+\tau_r p} i_{\mathrm{sd}} \tag{3-15}$$

$$\omega_{sl} = \frac{L_{\mathrm{m}}}{\tau_r} \frac{i_{\mathrm{sq}}}{\psi_{\mathrm{rd}}} \tag{3-16}$$

$$T_{em} = \frac{n_p L_m i_{\mathrm{sq}} \psi_{\mathrm{rd}}}{L_r} \tag{3-17}$$

In the formula： σ is the coefficient of magnetic leakage， $\sigma = 1 - \frac{L_{\mathrm{m}}^{\ 2}}{L_{\mathrm{r}} L_{\mathrm{s}}}$；

τ_r is the rotor time constant， $\tau_r = \frac{L_{\mathrm{r}}}{R_{\mathrm{r}}}$.

According to Equation (3-15), it can be seen that the amplitude of the rotor flux linkage is proportional to the d-axis component of the stator current; according to Equation (3-17), the torque is proportional to the q-axis component of the stator current when the rotor flux remains constant. Ignoring the cross-coupling term in Equations (3-13) and (3-14), the torque of the motor and the rotor flux can be controlled separately by controlling the dq-axis component of the stator voltage. The vector control method based on rotor magnetic field orientation can completely decouple the system, but the accuracy of this control strategy is affected by the motor parameters. Figure 3-3 shows the overall control block diagram of the motor system.

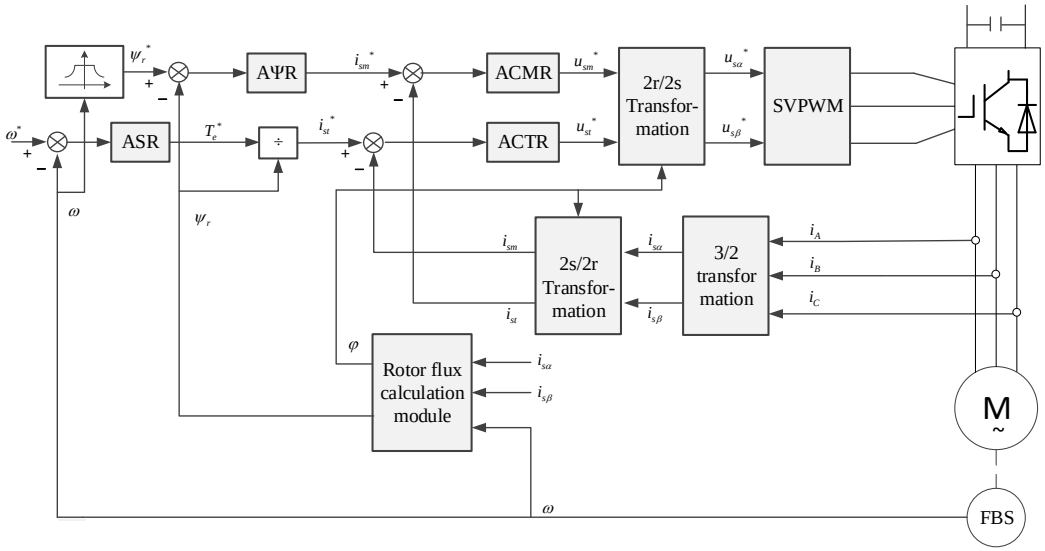

Fig. 3-3 The overall control block diagram of the motor system

Among them, ASR is the speed controller, AΨR is the flux linkage controller, ACMR is the excitation component of stator current controller, ACTR is the torque component of stator current controller, and FBS is the speed sensor. This article adopts a double closed-loop control system for the speed and flux linkage, in which the inner loop is current loop and the outer loops are speed loop and flux loop.

3.3 Controller Design of Vector Control System Based on Rotor Magnetic Field Orientation

The vector control system is a complex control system. In this section, the controller of the vector control system based on the rotor field orientation is designed, starting from the flux linkage loop and the speed loop. According to Equation (3-13) - Equation (3-17), the control block diagram of transfer function of the vector control system based on the rotor magnetic field orientation can be drawn, as shown in Figure 3-4.

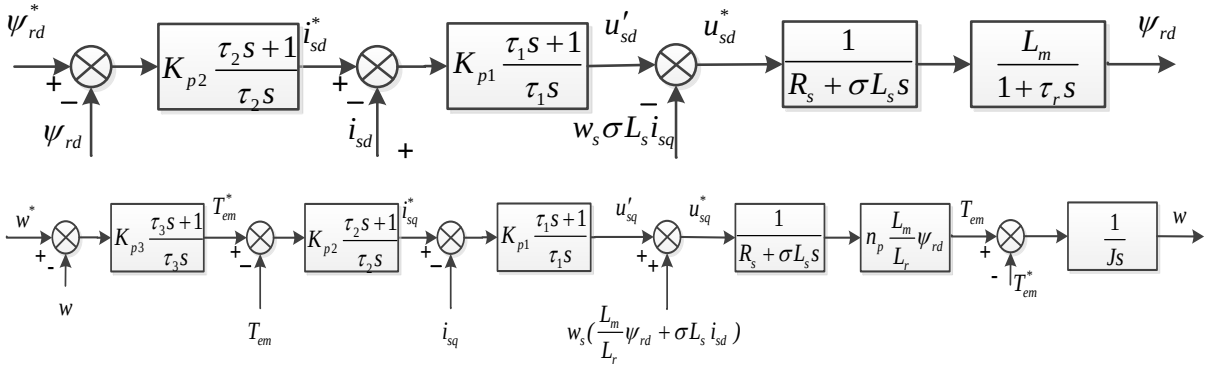

Fig. 3-4 Control block diagram of transfer function of the vector control system based on the rotor magnetic field orientation

3.3.1 Design of Flux Linkage Controller

According to Fig.3-4, the design of the flux linkage controller consists of two parts: the current inner loop and the flux linkage outer loop. The control goal of the flux linkage controller is to maintain the value of the rotor flux linkage constant and avoid the saturation of the flux linkage. The PI controller is used to design the current inner loop, and then the outer loop of the flux linkage is designed. Figure 3-5 is the control block diagram of the transfer function of current inner loop.

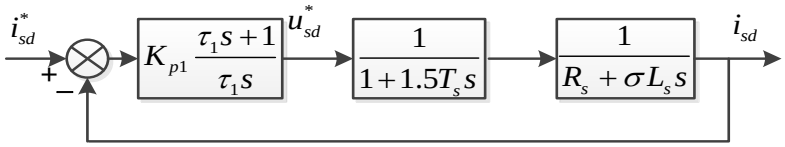

Fig. 3-5 Control block diagram of the transfer function of current inner loop

According to Figure 3-5, the open-loop transfer function of this subsystem is：

$$G_1(\mathrm{s}) = K_{p1}\frac{\tau_1 s+1}{\tau_1 s}\cdot\frac{1}{1+1.5T_s s}\cdot\frac{1}{R_s+\sigma L_s s} = \frac{K_{p1}(\tau_1 s+1)}{\tau_1 s(1+1.5T_s s)(R_s+\sigma L_s s)} \tag{3-18}$$

In the formula: $\mathrm{R}_s = 1.405; \mathrm{R}_r = 1.395; L_m = 0.1722; L_s = L_r = 0.181; \sigma = 0.095; T_s = 6.67\times10^{-5}$;

Let $\tau_1 = \frac{\sigma L_s}{R_s} = 0.012$, and the transfer function of this subsystem is：

$$G_1(\mathrm{s}) = \frac{K_{p1}}{\tau_1 R_s s(1+1.5T_s s)} \tag{3-19}$$

According to Equation (3-19), the transfer function is in line with a typical type I system and it should be set according to the second-order optimal model.

Let $\frac{K_{p1}}{\tau_1 R_s}\cdot 1.5T_s = 0.5$, and it can be obtained： $K_{p1} = \frac{0.5\tau_1 R_s}{1.5T_s} = 84.3, K_{i1} = \frac{K_{p1}}{\tau_1} = 7025$.

Equations (3-20) and (3-21) are the open-loop transfer function and closed-loop transfer function of this subsystem at this point.

$$G_1(\mathrm{s}) = \frac{5000}{s(1+1.5T_s s)} \tag{3-20}$$

$$G_{c1}(\mathrm{s}) == \frac{G_1(\mathrm{s})}{1+G_1(\mathrm{s})} = \frac{5000}{s(1+1.5T_s s)+5000} \tag{3-21}$$

Figure 3-6 shows the frequency response characteristics of the open loop logarithm of the current inner loop. It can be seen that it crosses the zero point with a slope of -20dB/dec and has a certain width, so the system is stable.

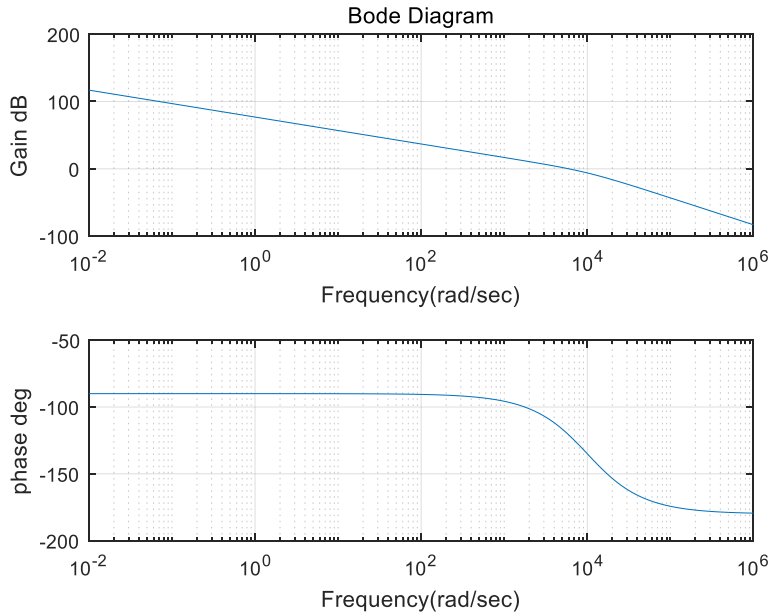

Fig. 3-6 Frequency response characteristics of the open loop logarithm of the current inner loop

Next, the controller parameters of the outer loop of the flux linkage should be designed. Figure 3-7 shows the control block diagram of transfer function of the flux linkage outer loop.

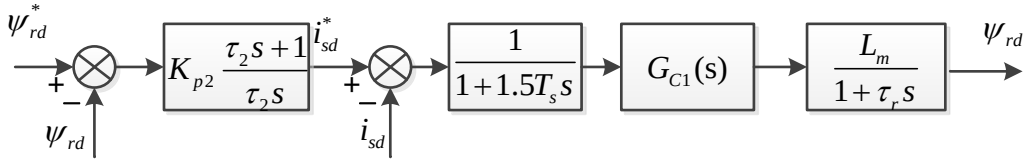

Fig. 3-7 Control block diagram of the transfer function of the flux linkage outer loop

According to Figure 3-7, the closed-loop transfer function of this system can be approximated as：

$$G_2(s) = K_{p2}\frac{\tau_2 s+1}{\tau_2 s}\cdot\frac{1}{1+1.5T_s s}\cdot G_{C1}(s)\cdot\frac{L_m}{1+\tau_r s} \approx \frac{K_{p2}L_m(\tau_2 s+1)}{\tau_2 s[1+(1.5T_s+\frac{1}{5000})s](1+\tau_r s)} \tag{3-22}$$

Let $\tau_2 = \tau_r = \frac{L_r}{R_r} = 0.13$， and the transfer function of this subsystem is：

$$G_2(s)=\frac{K_{p2}L_m}{\tau_2 s[1+(1.5T_s+\frac{1}{5000})s]} \tag{3-23}$$

According to Equation (3-23), the transfer function belongs to typical type I system and it should be set according to the second-order optimal model. Let $\frac{K_{p2}L_m}{\tau_2}\cdot(1.5T_s+\frac{1}{5000})=0.5$, and it can be obtained: $K_{p2}=\frac{0.5\tau_2}{(1.5T_s+\frac{1}{5000})L_m}=1258, K_{i2}=\frac{K_{p2}}{\tau_2}=9676$.

Figure 3-8 shows the frequency response characteristics of the open loop logarithm of the flux linkage outer loop. It can be seen that it crosses the zero point with a slope of -20dB/dec and has a certain width, so the system is stable.

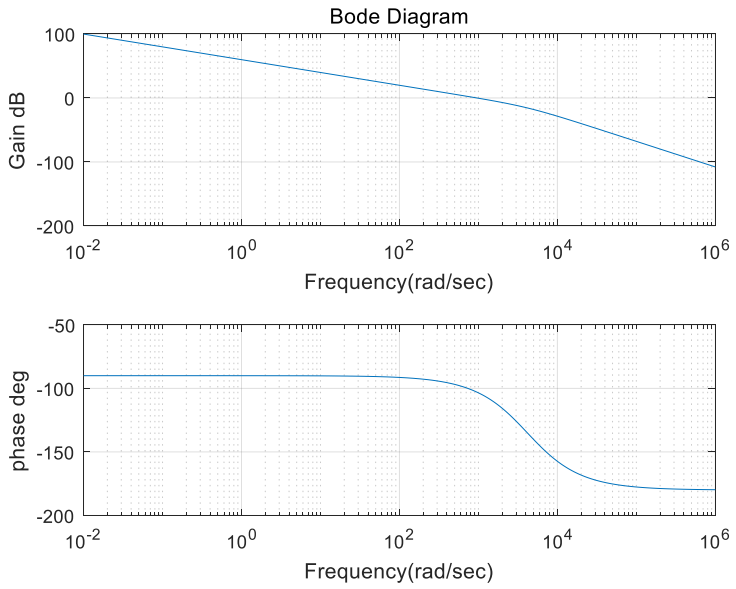

Fig. 3-8 Frequency response characteristics of the open loop logarithm of the flux linkage outer loop

3.3.2 Design of Speed Controller

According to Figure 3-4, it can be seen that the design of the speed controller is divided into three parts: speed outer loop, torque inner loop and current inner loop. The control target of the speed controller is to adjust the speed of the motor, and guarantee that the speed control system has excellent dynamic and static characteristics. The design method is still from the design of the inner loop, and then the design expands outward. Fig. 3-9 is the control block diagram of the transfer function of current inner loop. Its design of the

specific parameters and the design of the current inner-loop parameter in the flux linkage controller are exactly the same. It can be obtained: $K_{p1}=\frac{0.5\tau_1 R_s}{1.5T_s}=84.3, K_{i1}=\frac{K_{p1}}{\tau_1}=7025$.

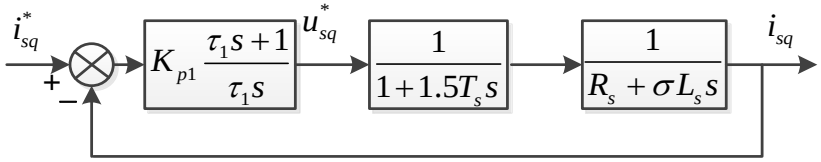

Fig. 3-9 Control block diagram of the transfer function of the current inner loop

Next, the relevant parameters of the torque inner loop should be designed. Figure 3-10 shows the control block diagram of the transfer function of the torque inner loop. n_p is the motor pole pair number, which is equal to 2 in this paper. According to Figure 3-10, the open-loop transfer function of this subsystem can be obtained, as shown in Equation (3-24).

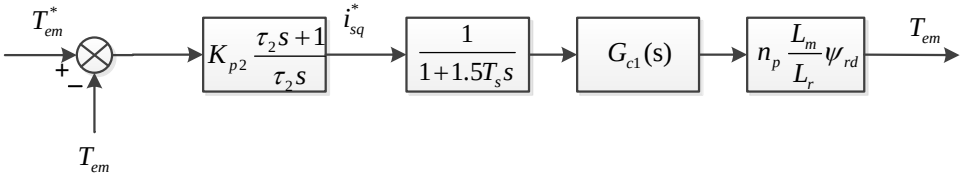

Fig. 3-10 Control block diagram of the transfer function of the torque inner loop

$$G_2(s)=K_{p2}\frac{\tau_2 s+1}{\tau_2 s}\cdot\frac{1}{1+1.5T_s s}\cdot G_{C1}(s)\cdot n_p\frac{L_m}{L_r}\psi_{rd}\approx\frac{K_{p2}n_p\psi_{rd}L_m(\tau_2 s+1)}{\tau_2 L_r s(1+1.5T_s s)(1+\frac{1}{5000}s)} \quad (3\text{-}24)$$

Let $\tau_2=\frac{1}{5000}$, and the transfer function of this subsystem is：

$$G_2(s)=\frac{K_{p2}n_p\psi_{rd}L_m}{\tau_2 L_r s(1+1.5T_s s)} \quad (3\text{-}25)$$

According to Equation (3-25), the transfer function belongs to typical type I system and it should be set according to the second-order optimal model. Let $\frac{K_{p2}n_p\psi_{rd}L_m}{\tau_2 L_r}\cdot 1.5T_s=0.5$, and it can be obtained： $K_{p2}=\frac{0.5\tau_2 L_r}{1.5T_s n_p\psi_{rd}L_m}=0.66, K_{i2}=\frac{K_{p2}}{\tau_2}=3285$. Equations (3-26)

and (3-27) are the open-loop transfer function and closed-loop transfer function of this subsystem at this time.

$$G_2(s) = \frac{5000}{s(1+1.5T_s s)} \tag{3-26}$$

$$G_{c2}(s) = \frac{G_2(s)}{1+G_2(s)} = \frac{5000}{s(1+1.5T_s s)+5000} \tag{3-27}$$

Figure 3-11 shows the frequency response characteristics of the open loop logarithm of the torque inner loop. It can be seen that it crosses the zero point with a slope of -20dB/dec and has a certain width, so the system is stable and has strong anti-interference performance.

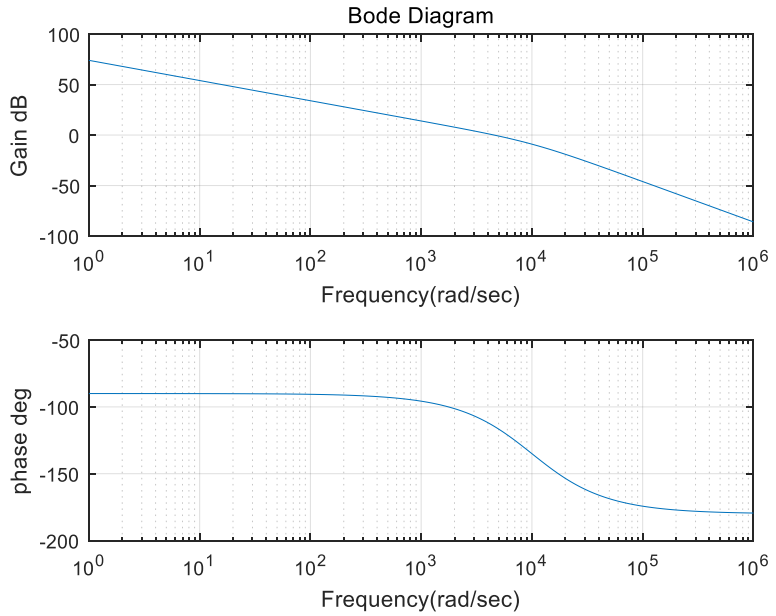

Fig. 3-11 Frequency response characteristics of the open loop logarithm of the torque inner loop

Lastly, the relevant parameters of the speed outer loop should be designed. Figure 3-12 shows the control block diagram of the transfer function of the speed outer loop.

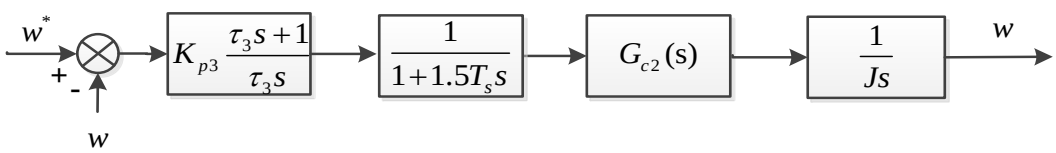

Fig. 3-12 Control block diagram of the transfer function of the speed outer loop

According to Figure 3-12, the closed-loop transfer function of this system can be approximated as：

$$G_3(s)=K_{p3}\frac{\tau_3 s+1}{\tau_3 s}\cdot\frac{1}{1+1.5T_s s}\cdot G_{c2}(s)\cdot\frac{1}{Js}\approx\frac{K_{p3}(\tau_3 s+1)}{\tau_3 Js^2[1+(1.5T_s+\frac{1}{5000})s]} \tag{3-28}$$

J is the rotational inertia of the asynchronous motor, which is taken as =0.0094 kg.m^2. According to Equation (3-28), the transfer function is in accordance with a typical type II system. According to the typical type II system parameter tuning method, if the intermediate frequency bandwidth parameter *h* is equal to 5, it can be obtained：

$$\begin{cases}\tau_3=h(1.5T_s+\dfrac{1}{5000})\\ \dfrac{K_{p3}}{\tau_3 J}=\dfrac{h+1}{2h^2(1.5T_s+\dfrac{1}{5000})^2}\end{cases} \tag{3-29}$$

At this point, K_{p3} is equal to 18.8 and K_{i3} is equal to 12533. Figure 3-13 shows the frequency response characteristics of the open loop logarithm of the speed outer loop. It can be seen that it crosses the zero point with a slope of -20dB/dec, which has a large stability margin and strong anti-interference performance. Therefore, the system is stable.

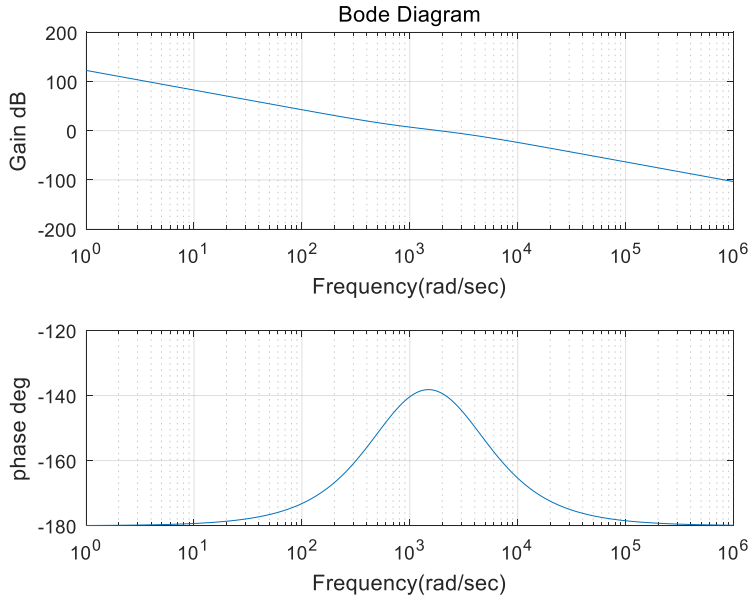

Fig. 3-13 Frequency response characteristics of the open loop logarithm of the speed outer loop

In summary, the flux linkage controller and speed controller of the vector control system based on rotor magnetic field orientation have been designed. In the process of design of the controllers, some polynomials are mathematically approximated. Therefore, in the simulation and the actual test platform debugging, the relevant parameters are adjusted within a certain range based on the actual situation and past experience, which realizes an excellent control effect.

3.4 Summary

This chapter firstly introduces the mathematical model of the asynchronous motor, and then introduces the basic principle of the vector control system based on the rotor magnetic field orientation, and finally completes the design of the flux linkage controller and the speed controller. Besides, the stability of the controllers is verified.

.

4 EXPERIMENT ANALYSIS OF MUTUAL FEEDBACK AC DRIVE TEST SYSTEM

4.1 Simulation Analysis of Mutual Feedback AC Drive Test System

In order to verify the feasibility of the design of the mutual feedback AC drive test system, the Simulink simulation platform of Matlab software is adopted to complete the simulation verification of the system.

Table 6-1 is the index of single-phase PWM rectifier.

Table 6-1 Index of single-phase PWM rectifier

Parameter	Reference value	Parameter	Reference value
Rated power	4.5kW	Efficiency	≥ 0.8
Input voltage	220（1±10%）VAC	Power factor	≥ 0.95
Input Voltage Frequency	50Hz	Output voltage ripple factor	$\leq 1\%$

Table 6-2 is the related parameters of the mutual feedback AC drive test system.

Table 6-2 Parameters of the mutual feedback AC drive test system

Parameters of single-phase PWM rectifier			
Input voltage	220V	Energy storage capacitor	5000μF
Input inductance	4mH		
Parameters of asynchronous motor			
Rated power	4kW	Stator resistance	1.405Ω
Rated speed	1440r/min	Rotor resistance	1.395Ω
Rated torque	25.4Nm	Magnetizing inductance	0.1722H
Rated line voltage	380V/50Hz	Stator rotor leakage resistance	5.8mH
Moment of inertia	0.0094kg.m^2	Number of pole pairs	2

4.2 Simulation Analysis of Single-phase PWM Rectifier

The simulation model of the mutual feedback AC drive test system is shown in Fig.4-1. The main circuit includes two symmetrical single-phase PWM rectifiers, two three-phase inverters and a pair of coupled asynchronous motors. The amplitude of the AC voltage source is 311V and the frequency is 50Hz, which simulates the actual grid voltage. The AC power is rectified by the PWM rectifier to access the three-phase converter to drive the asynchronous motor. Among them, one motor works in the electric state and the other motor works in the state of power generation. In this paper, the simulation steps are 1e-6s.

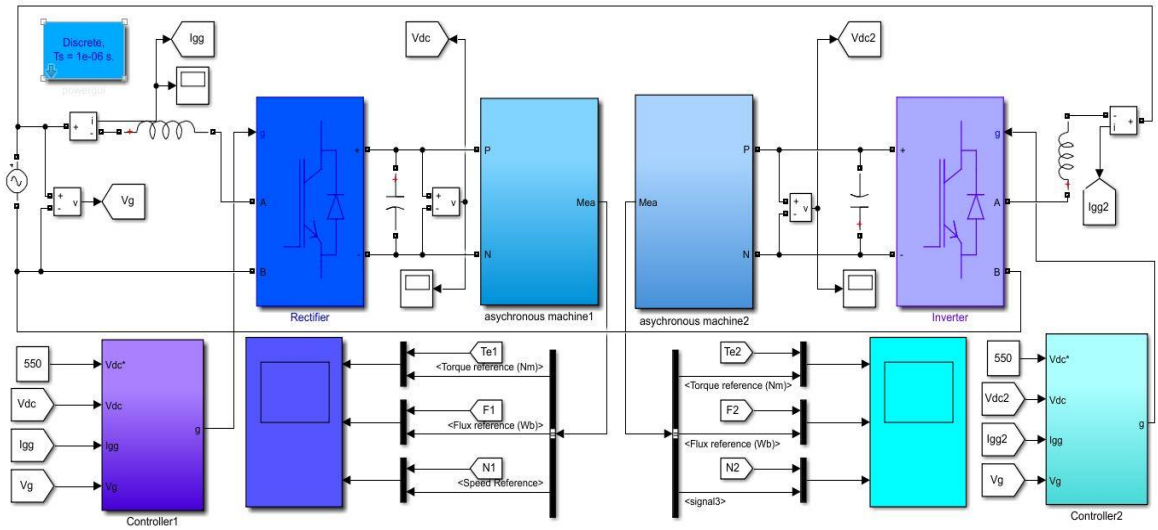

Fig. 4-1 Simulation model of the mutual feedback AC drive test system

First of all, the simulation of the single-phase PWM rectifier is verified. As shown in Fig.4-2, the single-phase PWM rectifier is simulated using three control strategies: PI control, proportional resonance control, and repetitive control. The command value of the DC-side voltage in this paper is 550V, and the DC-side bus voltage waveform can be obtained. It can be seen that the stable DC-side busbar voltage can be obtained quickly with these three control strategies. As shown in Fig.4-2, it can be seen that when adopting PR control, the overshoot of the system is too large. Because in the actual project, adopting PI control can not control the AC system without difference which is possible to cause the breakdown of the system, so this paper adopts repetitive control to control single-phase PWM rectifier.

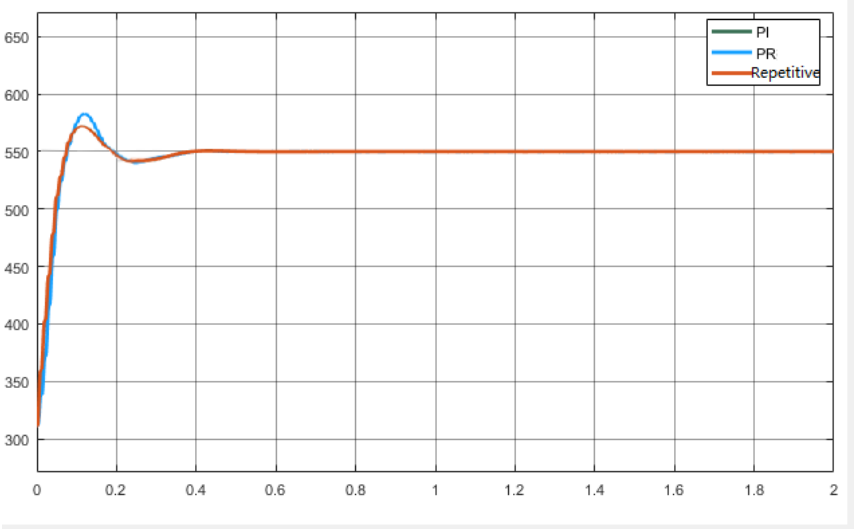

Fig. 4-2 DC-side busbar voltage of the PWM rectifiers with three control strategies

For the control of single-phase PWM converter, on the one hand it requires the stable DC voltage, on the other hand it requires the AC side can achieve unity power factor operation, at the same time, it need to minimal harmonic currents on the AC side.

Assuming that the load side of the rectifier is connected to a 100Ω resistor, as shown in Fig.4-3. It can be seen that the phase of grid voltage is as same as the input current, with good dynamic performance and steady-state accuracy, which meets the expected goals of the simulation.

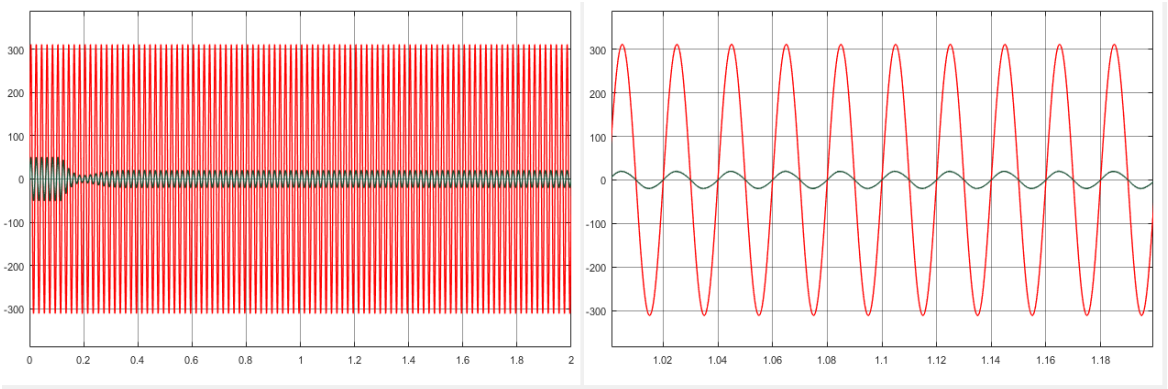

（a）0~2s （b）Steady state（1.0~1.2s）

Fig. 4-3 Grid voltage and input current of the PWM rectifier

When the resistance on the load side is 100Ω, Fourier analysis of the grid current is performed. As shown in Fig.4-4, the THD(Total Harmonic Distortion) of the system is 3.15%. It shows that the control effect of the PWM rectifier is obvious and the harmonics are effectively suppressed.

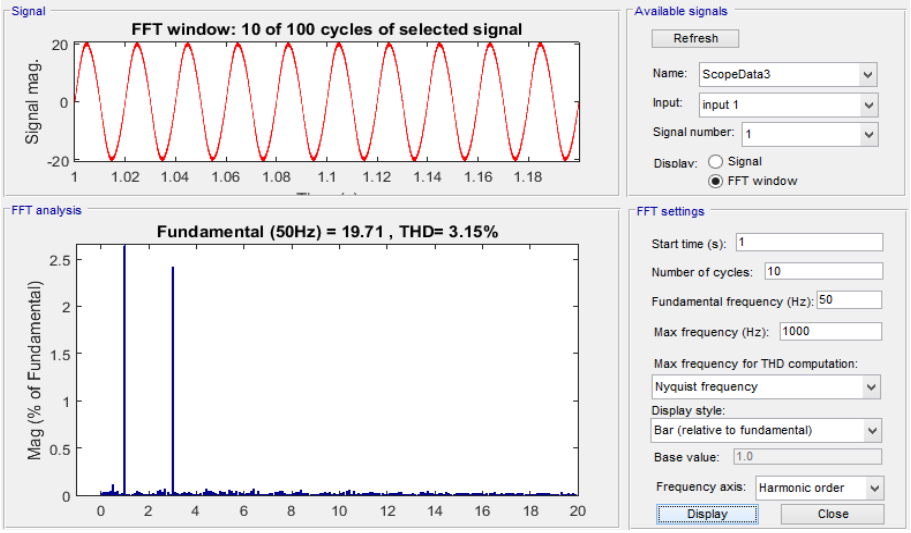

Fig. 4-4 Fourier analysis of the grid current

4.2.1 Simulation Analysis of Vector Control System Based on Rotor Magnetic Field Orientation

Next, the design of the vector control system is verified by simulation. The first thing to consider is the conditon on the sudden change of load of the motor. The specific steps are as follows: the single-phase PWM rectifiers on both sides are started, the stable 550V voltage is established on the DC side of the PWM rectifier, and the asynchronous motor 1 is started with no load at 2s. At 3s the asynchronous motor 2 is loaded to 25Nm and the load of the asynchronous motor 2 is reduced to 15Nm at 4s.

The asynchronous motor firstly raises the speed to 1300 r/min by the ramp speed function, and the slope of the ramp function is 2000 rpm/s. During the operation of the system, the motor speed remains unchanged after reaching the command value of 1300r/min. Fig.4-5 shows the speed waveforms of the asynchronous motor 1 and the asynchronous motor 2.

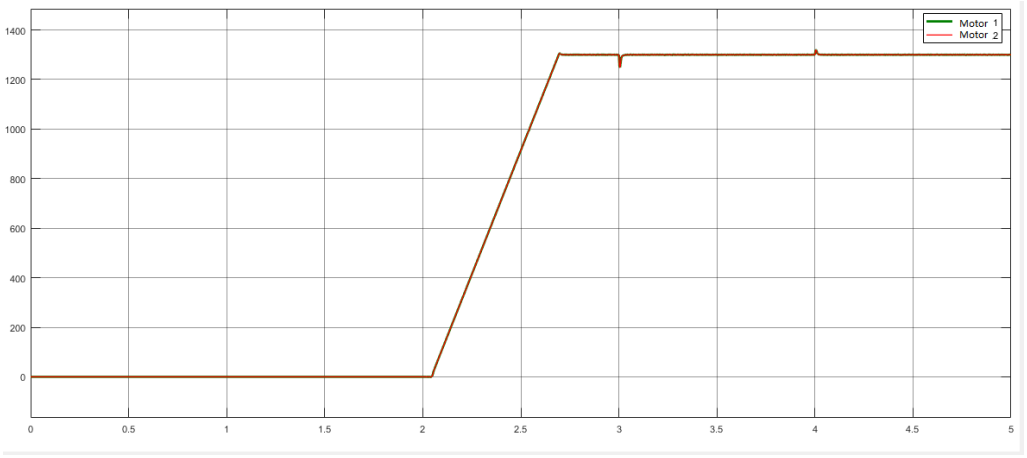

Fig. 4-5 Speed waveform of the asynchronous motor

It can be seen that the speed tracking effect of the motor is good. The asynchronous motor reaches a given speed around 2.7s. After the speed is stable, it basically achieves no static error with good dynamic performance and steady state characteristics.

Accurate observation and control of the flux linkage is the key to motor speed regulation. In this paper, the command value of the flux linkage is 0.8. As can be seen from Fig.4-6, the flux linkage control effect of the system is good, and the decoupling control of excitation current and torque current is effectively achieved.

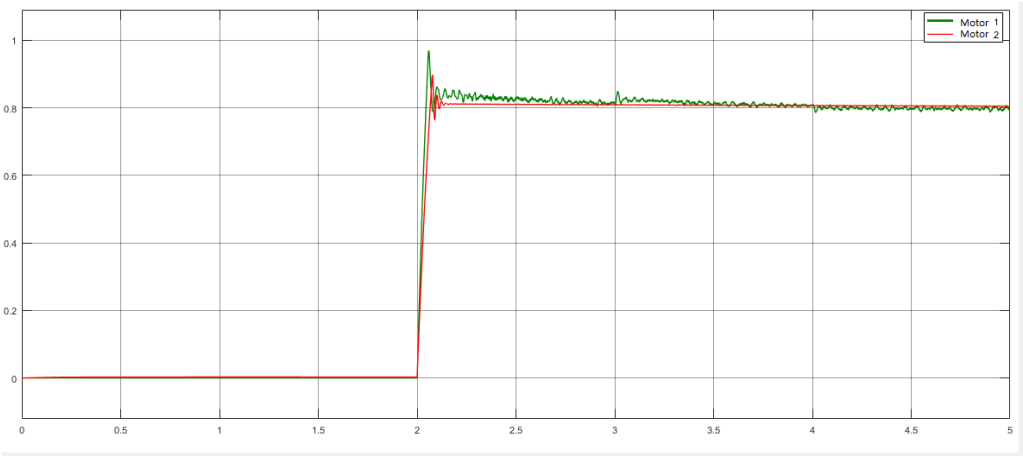

Fig. 4-6 Linkage waveform of the asynchronous motor

As shown in Fig.4-7, the torque of the asynchronous motor 1 suddenly increases and quickly stabilizes to about 25Nm at 3s. At 4s, the torque suddenly decreases and rapidly stabilizes at around 15Nm. The electromagnetic torque has a good tracking effect to the load torque which is in full compliance with expectations. Similarly, asynchronous motor 2 also has a good torque control effect.

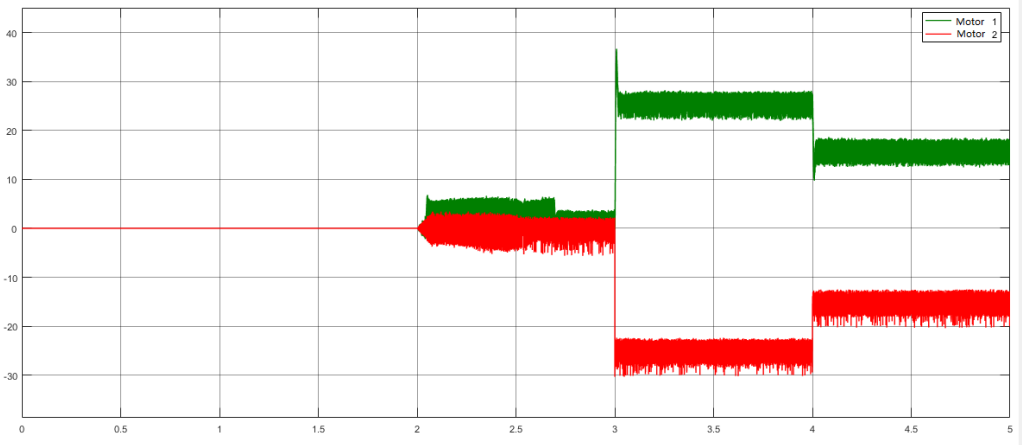

Fig. 4-7 Torque waveform of the asynchronous motor

On the other hand, it is necessary to simulate the speed regulation capability of the asynchronous motor. In this case, only the speed and torque characteristics of a single motor need to be analyzed. First of all, stable voltage is established on the DC side of the PWM rectifier, and the asynchronous motor starts without load at 2s. At this point, the speed of the motor is increased by the ramp function to 1000r/min, and the speed command value is increased to 1300r/min at 3s. And the speed command value is reduced to 600r/min at 4s. The load torque of the asynchronous motor is maintained at zero during the entire process.

As shown in Figure 4-8, the speed of the asynchronous motor can quickly follow the command value. It can be seen that the system has a good speed control effect. The overshoot of the flux linkage of the motor is very small and the flux linkage can quickly stabilize to the command value of 0.8. The electromagnetic torque of the motor also changes with the rotation speed. When the motor speed increases, the asynchronous motor will generate a larger positive electromagnetic torque, and then return to zero torque after the rotation speed is stable; When the motor speed drops, the asynchronous motor will produce a large reverse electromagnetic torque and return to zero torque after the speed stabilizes. In summary, the mutual feedback AC test system has excellent speed control capability.

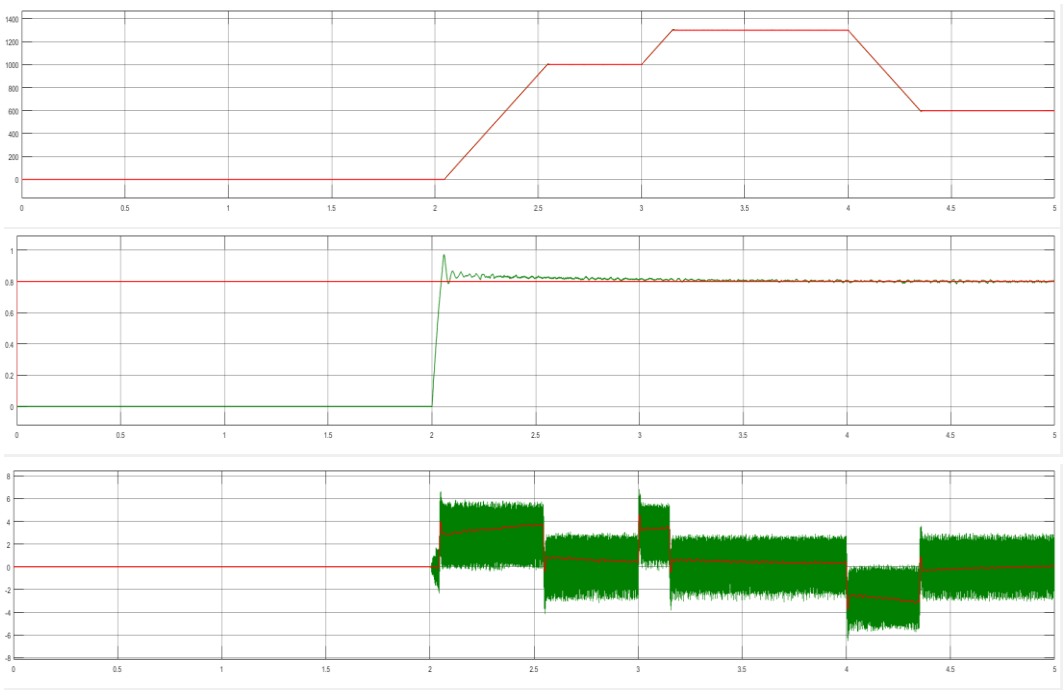

Fig. 4-8 Operating conditions of asynchronous motor (speed, flux linkage and torque)

In the vector control system based on the rotor field orientation, the dynamic characteristics and steady state performance of the asynchronous motor are the key indicators for measuring system performance and capability. From the simulation results of the vector control system, it can be seen that the control effect of speed, torque and flux linkage of asynchronous motor is good. Besides, it can accurately follow the command value, in line with the expected simulation goals.

4.2.2 Simulation Analysis of Energy Feedback

In a complete mutual feedback AC drive system, the asynchronous motor 1 operates in an electric state, and the asynchronous motor 2 operates in a power generation state. The mechanical energy generated by the asynchronous motor 2 is fed back to the DC bus side through the converter, and then the energy is fed back to the power grid. At the same time, energy is supplied to the motor to realize energy feedback. This section considers the sudden load change of the motor, that is, asynchronous motor 1 starts at 2s without load, loaded to 25Nm at 3s and loaded to 15Nm at 4s. When the motor speed reaches the command value ,it will keep constant in the whole process.

From the perspective of the electromagnetic torque of asynchronous motor, it can be seen from Fig.4-7 that at the stage of 3-5s, the electromagnetic torque of the asynchronous motor 1 in the electric state is positive. The asynchronous motor 2 works in the power generation state and the electromagnetic torque is a negative value, realizing the energy feedback between the asynchronous motor 1 and the asynchronous motor 2.

From the perspective of the relationship between the input current and the grid current of the PWM rectifier on both sides, the amplitude of the electric current should be the sum of the amplitudes of the grid current and the feedback current when the energy is fed back, and the phase of the electric current and the feedback current are opposite, same as grid current. When the PWM rectifiers are started, the amplitude and fluctuation of the current are relatively large. There is a fluctuation when the asynchronous motor 1 is started, and the amplitude also changes when the load torque suddenly changes.

Fig.4-9 shows the steady-state waveforms of the grid-side current, the electric current, and the feedback current when the load is 25Nm and 15Nm, respectively. From Fig.4-9, the amplitude of the electric current of the system is approximately the sum of the amplitudes of the grid-side current and the feedback current. The phase of the electric current and the

grid-side current are the same, and the phase difference from the feedback current is 180 °. And the amplitude of the current decreases as the load decreases.

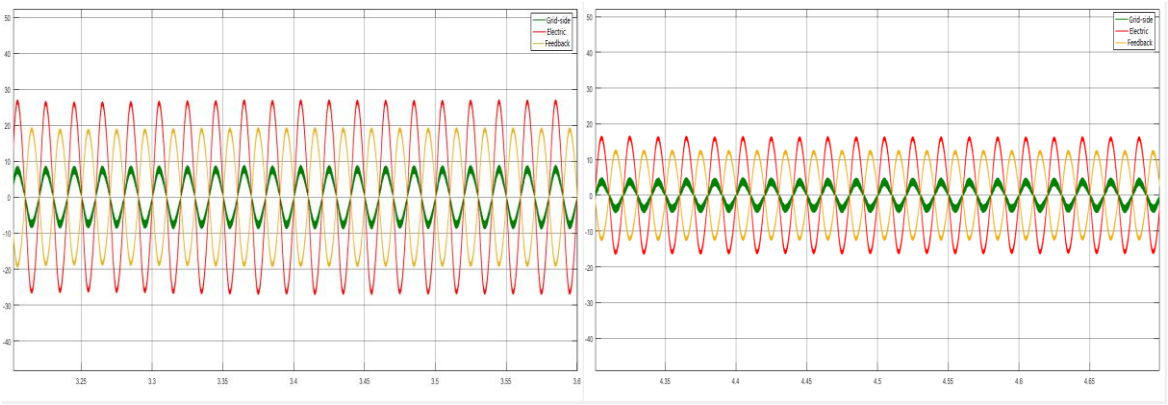

（a）Loaded to 25Nm　　（b）Loaded to 15Nm

Fig. 4-9 Steady-state waveforms of the grid-side current, the electric current, and the feedback current

4.3 Experiment Analysis of Mutual Feedback AC Drive Test System

The physical picture of the mutual feedback AC drive test system is shown in Fig.4-10.

Fig. 4-10 Physical picture of the mutual feedback AC drive test system

4.3.1 Experiment Analysis of Single-phase PWM Rectifier

First experiment is to verify the ability of the single-phase PWM rectifier to regulate the

DC bus voltage. As shown in Figure 4-11, channel 2 is the DC voltage and channel 3 is the input current. With the start of the PWM rectifier, the voltage on the DC side rises smoothly, stabilizing near the command value of 550V, and the overshoot is approximately zero. The amplitude of the input current increases as the DC side voltage increases, and stabilizes when the DC side voltage stabilizes.

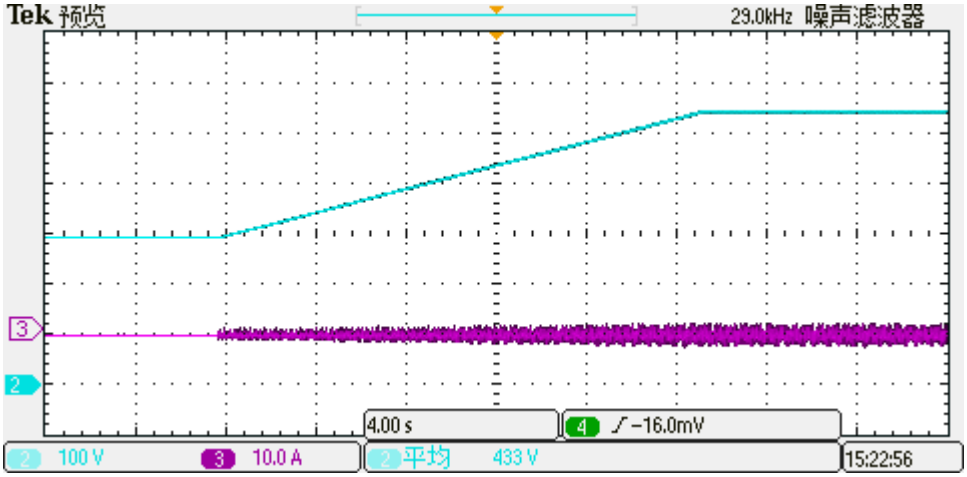

Fig. 4-11 DC-side busbar voltage of the PWM rectifiers

DC-side voltage is an important indicator to measure the performance of single-phase PWM rectifier. However, due to the limited observation time of the oscilloscope, it is not possible to intuitively provide waveforms when the DC-side voltage changes within a relatively large time range. Therefore, in order to examine the steady-state characteristics of the DC-side voltage, this paper records its waveform on the host computer, as shown in Figure 4-12. From Figure 4-12, it can be seen that the voltage on the DC side rapidly reaches the command value of 550V, the overshoot is approximately zero, and the steady-state performance is good.

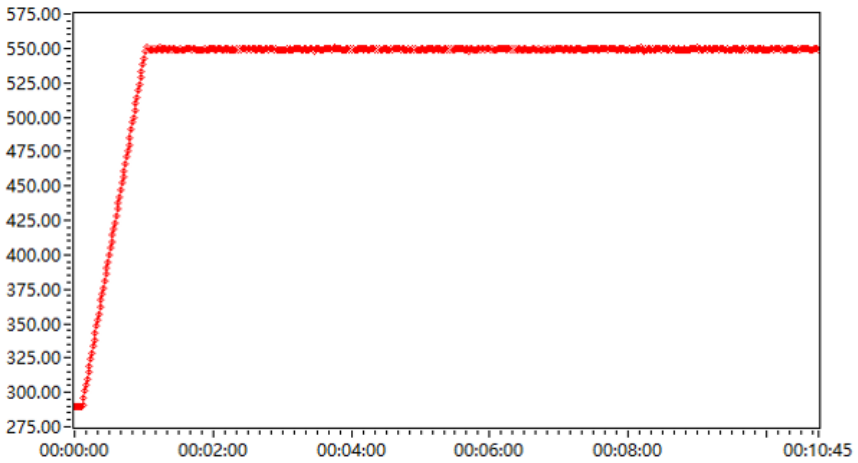

Fig. 4-12 DC-side busbar voltage of the PWM rectifiers

For the control of single-phase PWM rectifier, on the one hand it requires the stable bus voltage on the DC side, on the other hand it requires that the AC side can achieve unity power factor operation, and it requires the AC side of the harmonic current is very small. Figure 4-13 shows the steady-state operating conditions of the single-phase PWM rectifier with 100Ω at different voltage levels.

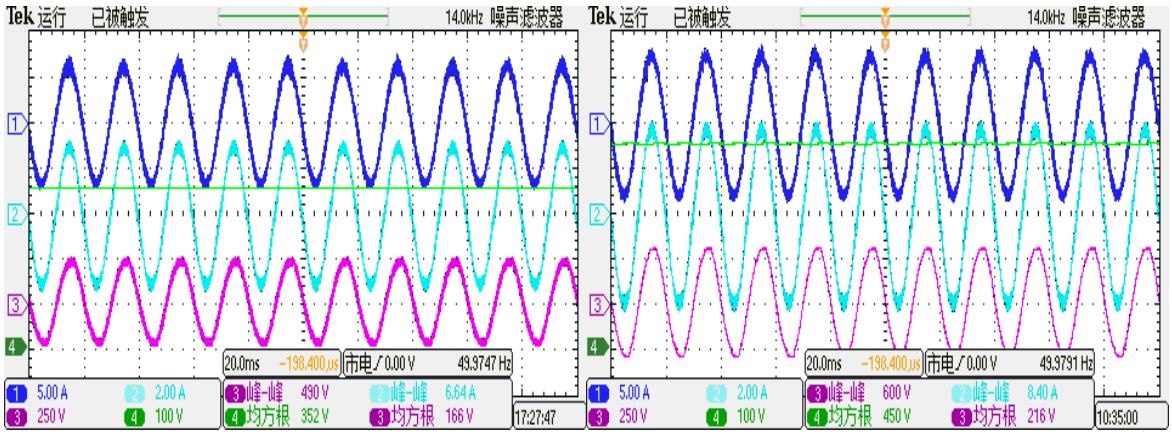

（a）DC voltage command value is 350V （b）DC voltage command value is 450V

Fig. 4-13 Steady-state operating conditions of the single-phase PWM rectifier with 100Ω at different voltage levels

As shown in Figure 4-13, channel 4 is the DC side voltage. It can be seen that the DC side voltage of the PWM rectifier is stable at 352V and 450V respectively; channel 2 is the load current, and channel 1 and channel 3 are the grid side currents and grid voltage respectively. It can be seen that the grid-side current and the grid voltage are in the same phase, the sinusoidal degree of the grid-side current is high, and the single-phase PWM rectifier basically realizes the grid-side unit power factor.

4.3.2 Experiment Analysis of Vector Control System Based on Rotor Magnetic Field Orientation

550V voltage is established on the DC side of the single-sided PWM rectifier, and then the asynchronous motor 1 is started with no load, and then the motor speed reaches a given value of 1300r/min. As shown in Figure 4-14, channel 2 is the voltage on the DC side, channel 3 is the stator current of phase A of the asynchronous motor 1 during start-up, and channel 4 is the waveform of the observed magnetic flux. It can be seen that the asynchronous motor 1 starts smoothly, the stator current waveform is stable, and there is no overshoot; the flux linkage observation effect is good, and the command value is accurately followed, thereby ensuring the precise control of the excitation current and the torque current.

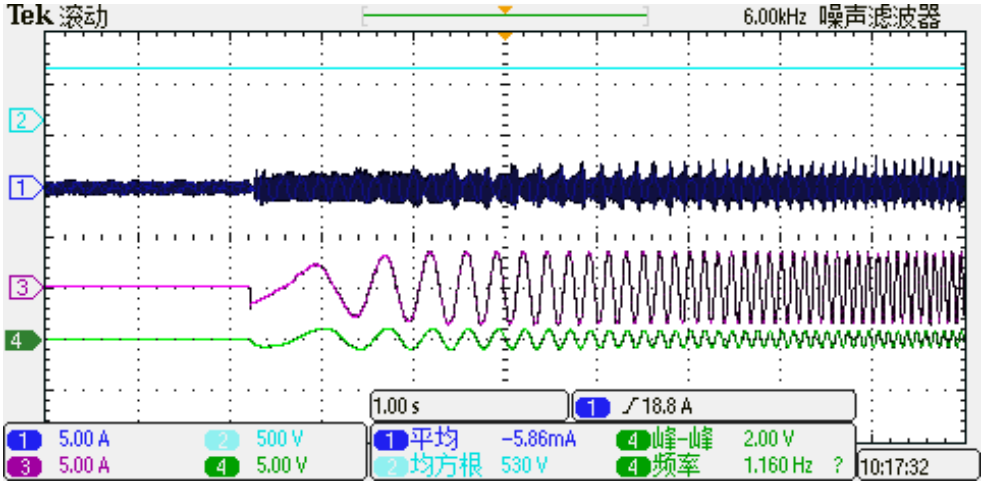

Fig. 4-14 Operating conditions of asynchronous motor 1

Next, the speed regulation capability of the asynchronous motor must be verified. The speed control capability of the motor is not only reflected in the rapidity of speed realization, but also reflected in the extensiveness of the speed range.

The observation considers the following conditions: The PWM rectifiers on both sides are activated, and the stable 550V DC side voltage is established at one minute and ten seconds, and then the asynchronous motor 1 and the asynchronous motor 2 are started successively. The initial speed command value of asynchronous motor 1 is 100r/min, and the speed of asynchronous motor 1 quickly reaches the command value 100r/min. At this time, when the system detects that the speed target has been achieved, the speed command value will increase by 100r/min, and the motor speed will increase immediately. The motor reaches the command value of 1300r/min in approximately 2 minutes and 40 seconds. At this point, the asynchronous motor 1 drags the asynchronous motor 2 to run. The motor runs at 1300r/min for two minutes, then the motor speed setpoint is reduced by 100r/min, similar to the acceleration process, and finally the motor speed is reduced to zero. Then the system switches the mode, and instead, the asynchronous motor 2 drives the asynchronous motor 1 to run and repeats the previous process.

As shown in Figure 4-15, it fully meets the desired target. The system has good speed control performance with high accuracy and high stability.

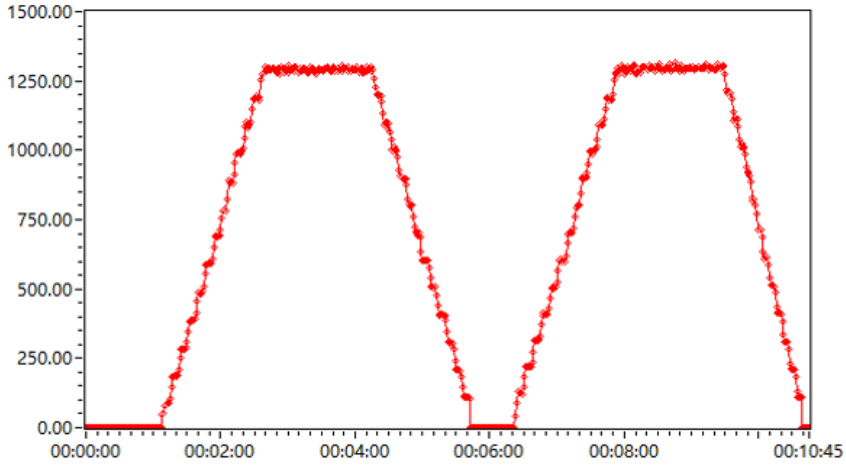

Fig. 4-15 Waveform of the speed of the asynchronous motor 1

Figure 4-16 shows waveform of the three-phase current of the stator-side when the speed of the asynchronous motor 1 decreases and then increases. As shown in the figure, the current of the stator side of the asynchronous motor is stable. The frequency of the current increases with the increase of the speed and decreases with the decrease of the speed. The frequency conversion effect is obvious and meets the expected target.

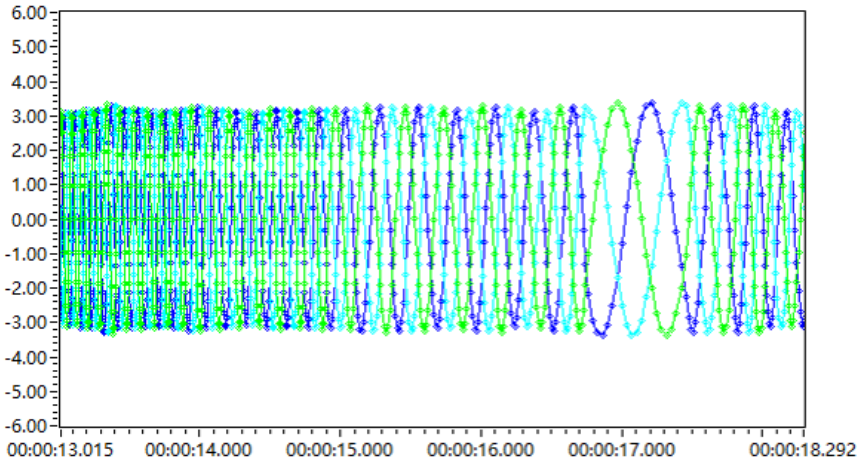

Fig. 4-16 Waveform of the three-phase current of the stator-side

4.3.3 Experiment Analysis of Energy Feedback

After completing the experimental verification of the two subsystems of single-phase PWM rectifier and vector control system, it is necessary to verify the overall energy-feedback function of the system. The specific steps are as follows: First, the PWM rectifiers on both sides are started. After the stable 550V voltage is established on the DC side, the asynchronous motor 1 and the asynchronous motor 2 are started one after another. After the motor speed reaches a given value of 1300r/min, the asynchronous motor 2 loads.

At this point, the asynchronous motor 1 is in electric state and the asynchronous motor 2 is in generating state.

Figure 4-17 shows the waveforms of the electric current and feedback current under different load torques. Among them, channel 1 is the feedback current, channel 2 is the electric current. From Fig.4-17, it can be seen that the sinusoidal degree of the system electric current and feedback current is high and the steady-state performance is good. With the increase of load torque, the amplitude of the electric current and feedback current also increases. The phase difference between the electric current and the feedback current is 180 °, which indicates that the system realizes energy mutual feedback. From Fig.4-17, it can be seen that the energy feedback rates of the system under four load torque conditions are 44%, 44%, 50%, and 47%, respectively.

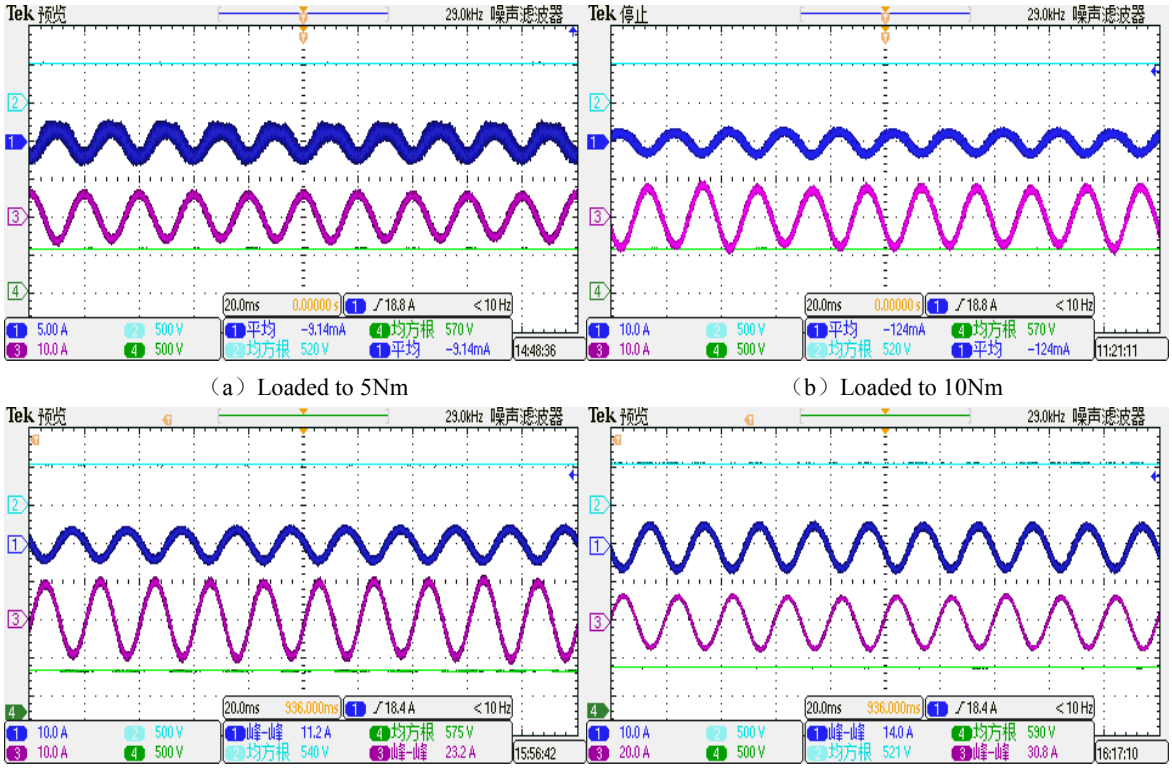

（a）Loaded to 5Nm　　（b）Loaded to 10Nm

（c）Loaded to 15Nm　　（d）Loaded to 20Nm

Fig. 4-17 Steady-state waveforms of the electric current and the feedback current

4.4 Summary

This chapter mainly introduces the simulation and experimental verification of the mutual feedback AC drive test system. Simulink simulation platform is adopted to verify the simulation from three aspects: single-phase PWM rectifier, vector control system and the

function of energy feedback. Finally, the previous system design and simulation are verified and analyzed experimentally. The experimental results fully meet the expected goals.

5 RESEARCH ON MONITORING DEVICE FOR MUTUAL FEEDBACK AC DRIVE TEST SYSTEM

5.1 Requirement of Monitoring Device

The mutual feedback AC drive test system is a complex, multi-variable and multi-link system, including the main circuit, control circuit, and host computer. The test system includes four converters and a pair of coupled motors. If a problem occurs in one part of the system, it is easy to cause the entire system to fail or even crash. This shows that the reliability of the system is very important. The monitoring device is a guarantee for the normal operation of the system. A complete monitoring device can greatly improve the stability and reliability of the system and reduce the maintenance cost. Therefore, the establishment of a complete monitoring device for the mutual feedback AC drive test system is of great importance.

PWM rectifier can obtain the stable DC-side voltage and guarantee the normal operation of the rear motor. Once the voltage on the DC side is unstable, it will have a direct impact on the operation of the asynchronous motor, and it may also cause pollution to the power grid. Therefore, monitoring of the PWM rectifier is indispensable.

The AC drive part is the core of the test platform. The speed and torque curve of the asynchronous motor is a standard to evaluate the performance of an AC drive test platform. However, under normal circumstances, it is difficult to observe the curve of the speed through conventional tools such as an oscilloscope, so the effect of host computer is highlighted at this time.

The control system of the mutual feedback AC drive test platform is very complicated, and the commutation link and the AC drive link influence each other. Therefore, the test platform has a high reliability requirement for each link. Through the host computer, the

parameters of the system can be observed and controlled. Once some parameters are abruptly changed, the host computer can spontaneously control the start-up and shutdown of the rectifier and motor units.

According to the overall structure and working principle of the above-mentioned mutual feedback AC drive test system, in combination with user requirements, the monitoring device of the mutual feedback AC drive test system needs to achieve the following functions:

a) Monitoring function: display the key parameters of each part of the mutual feedback AC drive test platform, such as voltage, current, speed, torque and power, to facilitate the observation for users;
b) Waveform drawing: display the characteristic curve of the speed torque, display the real-time waveform of voltage and current;
c) Data storage: record the historical data of the relevant parameters;
d) Real-time communication: complete communication between DSP and host computer and human-machine interface.

To sum up, the monitoring device of the mutual feedback AC drive test system must have strong anti-interference performance, data processing capability, reliability, stability, and be easy to maintain and operate.

5.2 Design of Monitoring Device

Fig.5-1 shows the block diagram of the monitoring device of the mutual feedback AC drive test system. As shown in the figure, based on the interface conditions of the actual main control board and human-machine interface, this test system designed two communication subsystems: one is the communication subsystem within the DSP board, ARM board and the host computer which is achieved by RS485 communication. The other one is the communication subsystem between the DSP and the human-machine interface, using the CAN communication mode (the RS232/485 serial port of the DSP board is occupied by the communication subsystem mentioned above, and the actual use of the human-machine interface does not have the CAN serial port,so it is exactly CAN to RS232 communication actually).

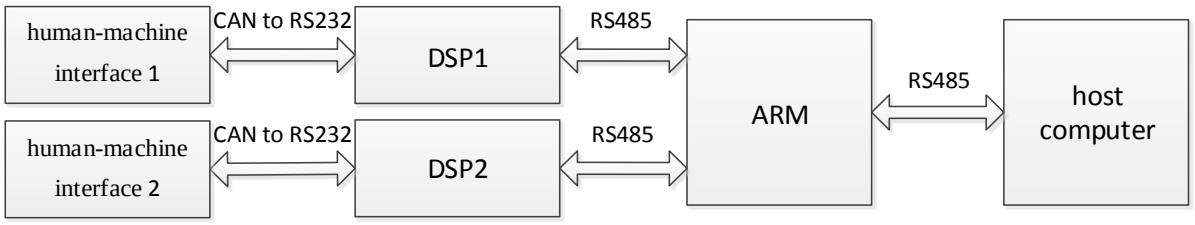

Fig. 5-1 Block diagram of the monitoring device of the test system

The low-power test platform adopts a two-level control scheme: that is, the ARM board is used to simulate the control of the CCU（Central Control Unit）, and the DSP board is used to simulate the control of the TCU(Transmission Control Unit). Each DSP board controls one TCU and there are two DSP board in this system.

5.3 CAN Communication Subsystem

5.3.1 Software Design

The experimental platform adopts CCS5.5 and MCGS(Monitor and Control Generated System) embedded version configuration software to complete the software design of the entire CAN communication subsystem. The DSP board is programmed in C language under the CCS5.5 environment and mainly completes the main program of the system and the communication interrupt service program. The MCGS software is mainly used to complete the interface design of the human-machine interface and the communication between the TPC7062Ti touch screen and the DSP board.

The communication mode of CAN bus adopts the mailbox structure. The mailboxes on each bus correspond to different addresses. Only the mailboxes with the same address can communicate. When data is sent, the processor distributes the data to individual mailboxes, and the data is sent to the matching mailbox on the target processor. After receiving the data in the mailbox, a corresponding interrupt request will be issued, waiting for the processor to read the action.

Because the human-machine interface actually used in this test platform does not have a CAN serial port, and the RS232/485 serial port of the main control board is occupied by another RS485 communication subsystem, so this article uses the CAN to RS232 communication method exactly. A CAN to RS232 communication protocol converter is necessary in this condition. This test platform uses the UT-2506 intelligent protocol

converter, as shown in Fig.5-2. UT-2506 intelligent protocol converter can connect RS232 serial port communication equipment to CAN bus.

Fig. 5-2 UT-2506 intelligent protocol converter

Usually the transmission baud rate of the CAN bus is about three times that of the RS232 serial port communication, so that the data transmission will be stable and less prone to errors. In this system, the CAN communication baud rate is 115200bps, and the serial baud rate is 38400bps.

The CAN bus uses a multi-master communication mode, and each node has the same status. RS232 communication is the master-slave communication mode. In this test platform, the human-machine interface is the host, and the DSP board is the slave, using the Modbus communication protocol. Modbus communication protocol is a universal protocol applied in the field of electronic device communication. With Modbus communication protocol, information communication between electronic devices can be realized. Modbus is a serial communications protocol originally published by Modicon (now Schneider Electric) in 1979 for use with its programmable logic controllers (PLCs). Modbus has become a de facto standard communication protocol and is now a commonly available means of connecting industrial electronic devices. In the communication process, the communication between the master device and the slave device will not affect the other actions of the system. What's more, it will not affect the other functions of the DSP board. This is an important factor in the adoption of the RS232 communication mode.

The communicaiton flowchart of the host and the slave is shown in Fig.5-3. After the host is initialized, the human-machine interface sends a data frame to the DSP board, waits for the reply from the machine, and repeats the cycle; At the same time, the slave waits for the command of the host. When it receives the data frame sent by the host, it firstly determines the slave address and function code. Then, the CRC check is performed. If the check is

correct, the corresponding palindrome is sent to the host. If the check fails, the host waits for the command again.

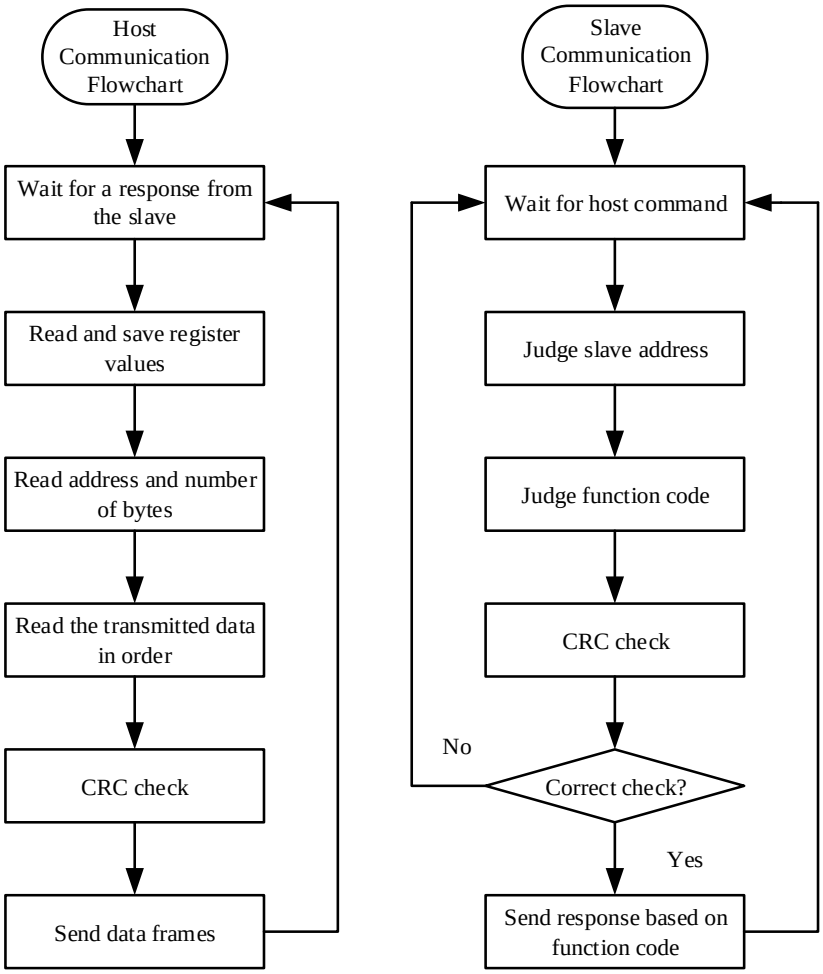

Fig. 5-3 Communicaiton flowchart of the host and the slave

5.3.2 Design of Human-machine Interface

TPC7062Ti touch screen produced by Beijing Kunluntongtai Automation Software Technology Co., Ltd is adopted in this article. It realizes data transmission between DSP board and human-machine interface through CAN to RS232 communication. TPC7062Ti is a high-performance embedded integrated touch screen based on Cortex-A8 processor. It has the advantages of strong transmission capability, high stability, low power consumption, and powerful image processing and data processing capability.

The human-machine interface is compiled by MCGS software. MCGS is a set of industrial control configuration software for the preparation of the host computer monitoring system. In this article, the following eight parameters are observed: grid voltage, grid current, DC

side voltage, input current, motor speed, motor torque, motor flux linkage, and motor stator current.

5.4 RS485 Communication Subsystem

The control signal is sent to the ARM board through the host computer. Then the ARM board performs calculation according to a specific algorithm and sends a control signal via the RS485 bus to control the DSP board of the converter 1 and the DSP board of the converter 2 respectively. At the same time, the ARM board transmits information to the host computer via the RS485 bus to realize human-machine interface information display.

The control software of the ARM board completes the overall coordination control function, and the DSP board completes the special control function of the converter. The main control programs of the two boards are both compiled in C language. The ARM board is based on the open source embedded Linux operating system. The DSP board program is compiled through CCS5.5. The host computer is compiled by Labview graphical programming software.

Although the RS485 communication also adopts the master-slave communication mode, the difference from the RS232 communication mode is that one host can correspond to multiple slaves for RS485 communication. Just as there are two DSP boards in this test platform, RS485 communication is adopted here. In the communication program between the DSP board and the ARM board, the ARM board is the master and the DSP board is the slave.

For data transmission, the low byte is sent first and the high byte is sent later; for a bit in a byte, the low bit is sent first, and then the high bit is sent again. With half-duplex asynchronous transmission, the baud rate is 9600 bps.

The ARM board sends self-check packet instructions, command packet instructions, and data packet instructions to the DSP board. The DSP board sends self-check packet instructions, data packet instructions, and command packet instructions to the ARM board.

The role of the self-check packet instruction is to check whether the control boards can communicate normally.The command packet sent by the ARM board is a request to the DSP board to send data. The data packet sent by the ARM board contains the operating

state of the converter and the command value of the relevant parameters of the motor. For the DSP board, the data packet represents the value of the relevant variable of the current converter and the motor unit, and the command packet it sends just indicate to the host that the packet sent by the host was received. The communicaiton flowchart of ARM board and DSP board is shown in Fig.5-4.

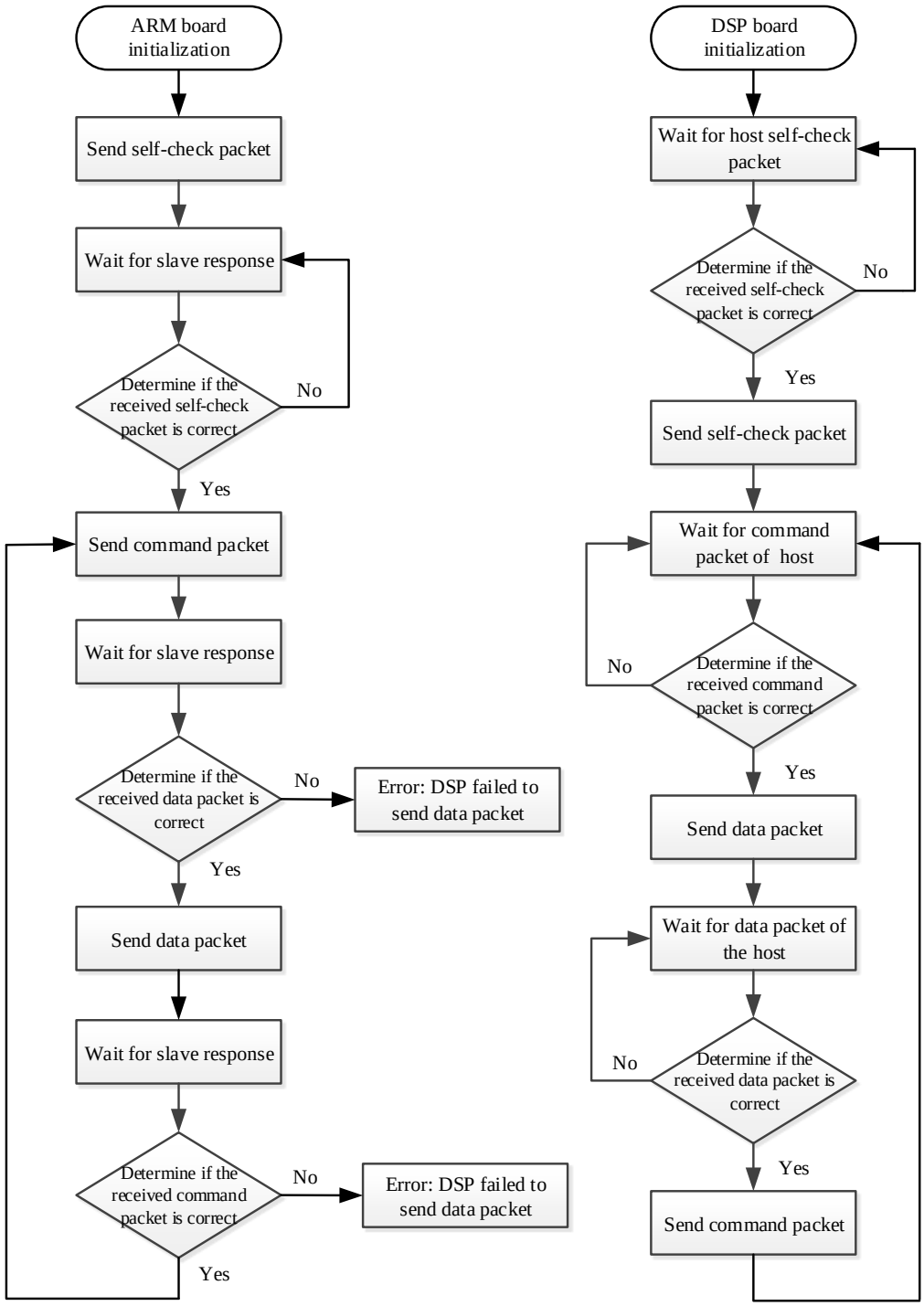

Fig. 5-4 Communicaiton flowchart of ARM board and DSP board

The specific communication flow is: After the program is initialized, the ARM board first sends the self-check packet to the DSP board, and then waits for the DSP board to respond. If the communication is successful, the DSP board will respond to the ARM board; otherwise, it will directly return to wait for the self-check packet of the ARM board. After the self-test is successful, the ARM board will send a command packet to the DSP board and wait for a response from the DSP. If the communication is successful, the DSP board will send a corresponding data packet to the ARM board; otherwise, an error will be reported. The ARM board will send data packets to the DSP board and wait for the response of DSP. If the communication is successful, the DSP board will send corresponding command packet to the ARM board; otherwise, an error will be reported. This communication process continues to cycle through.

5.5 Summary

This chapter first analyzes the requirements of the monitoring device of the mutual feedback AC drive test system, and then completes the design of the monitoring device. Finally, the software design of the CAN communication subsystem and the RS485 subsystem is completed, including the setting of the communication protocol and the communication flow.

6 CONCLUSION

6.1 Conclusion

The mutual feedback AC drive test system is a complex, multi-variable and multi-link system. The application of single-phase PWM rectifier technology improves power quality; the application of vector control technology greatly improves the dynamic performance and steady-state characteristics of the AC drive system, enabling energy feedback; adopting CAN bus technology and RS485 serial port communication technology realizes the monitoring and control of the entire system to ensure the stability of the system. In this paper, the Simulink simulation platform of Matlab software is adopted to establish a simulation model of the mutual feedback AC drive test system, and an actual test platform is built to verify the experiment. This proves the feasibility of the high-power AC drive test platform. Through the work of this article, the conclusions can be obtained as follows:

(1) The single-phase PWM rectifier technology based on repetitive control makes the system obtain the stable DC-side voltage, which effectively suppresses the current harmonics and improves the power quality.

(2) The vector control system based on rotor magnetic field orientation realizes the complete decoupling of the flux linkage and torque of the motor. Through building the model of the vector control system, the speed controller and flux linkage controller based on PI controller are completed. The design of the controller has good stability and has achieved a good control effect.

(3) The function of energy feedback of the mutual feedback AC drive test system is realized, in which one motor is in the electric state and one motor is in the power generation state. By analysing the phase and amplitude of the grid-side current, the electric

current, and the feedback current in the experiment, the energy feedback rate of the system can reach 50%.

(4) This paper has conducted in-depth analysis of the requirements of the monitoring device of the mutual feedback AC drive test system. Through RS485 serial port communication technology and CAN bus technology, monitoring device with strong anti-interference ability and high stability is established. It can realize monitoring function, data storage, waveform drawing and real-time communication, ensuring the stable operation of the mutual feedback AC drive test system.

6.2 Future research topics

Due to limited research time and limitations of my academic level, this paper can still make further improvements and research in the following areas:

(1) Although the vector control system based on the rotor magnetic field orientation realizes the complete decoupling of the motor flux linkage and the torque, it is sensitive to the parameters of the asynchronous motor. Therefore, in the subsequent studies, on the one hand, the control strategy can be improved; on the other hand, the test platform can add the function of the motor parameter identification, which will reduce the dependence of the system on the accuracy of motor parameters.

(2) Because the monitoring device adopts CAN bus communication technology and RS485 serial communication technology, the communication system is complex, and the test platform is a multi-link and multi-variable control system. The amount of program written into the DSP board is large. Therefore, in the subsequent studies, the communication protocol can be simplified, or the hardware system of the test platform can be optimized, and the speed of system data transmission can be improved.

7 REFERENCES

[1] B Mokrytzki. Filters for Adjustable Frequency Drives[C].Applied Power Electronics Conference and Exposition, 1994.

[2] S Gautam, R Gupta. Balanced Control of Multicell AC-DC Converter with Cascaded H-bridge Cells[C]. Electrical Computer and Electronics 2015 IEEE UP Section Conference, 2015.

[3] S Garg. Design and Analysis of Magnetic Levitation System by Using Memristor based Controller[C]. Magnetics Machines and Drives 2014 Annual International, 2014.

[4] Xiaopeng Dong, Zhaoan Wang. PWM Rectifier Control Based on Improved Cycle Average Model[J]. Power Electronics,1999(2):11-14.

[5] Liqun He, Jian Xiong, Hui Ouyang, Pengju Zhang, et al. High-Performance Indirect Current Control Scheme for Railway Traction Four-Quadrant Converters[J]. IEEE Transactions on Industrial Electronics, 2014, 61: 6645-6654.

[6] Chunjiang Zhang, Jing Zhang, Weiyang WU, et al. Delta Controller-based Resonant Controller for High-Frequency Inverter Waveform Control[J]. Transactions of China Electrotechnical Society, 2008,23(7):81-85.

[7] Chengzhi Wang, Yunping Zou, Yun Zhang, et al. Research on the Single-phase PWM Rectifier Based on the Repetitive Control[C]. Proceeding of IEEE International Conference on Industrial Technology, 2008.

[8] Chao Fu, Yuwei Sun, Kai Xu, et al. Single-phase PWM Rectifier Based on ADRC and PR Control[C]. Electrical Machines and Systems Conference, 2015:1884-1888.

[9] P Zanchetta, DB Gerry, VG Monopoli, et al. Predictive Current Control for Multilevel Active Rectifiers With Reduced Switching Frequency[J]. IEEE Transactions on Industrial Electronics, 2008, 55(1):163-171.

[10] R Nazir, A Wood, H Laird, et al. An Adaptive Repetitive Controller for Three-phase PWM Regenerative Rectifiers[C]. International Conference on Renewable Energy Research and Applications (ICRERA), 2015.

[11] Wensheng Song, Zhixian Deng, Shunliang Wang, et al. A Simple Model Predictive Power Control Strategy for Single-Phase PWM Converters With Modulation Function Optimization[J]. IEEE Transactions on Power Electronics, 2016,31:5279-5289.

[12] Kaizheng Huang, Wanwei Wang, Xu Wang. Modeling and Simulation of PWM rectifier Based on Sliding Mode Control[J]. Power System Technology, 2009, 33(8): 18-23.

[13] Heping Liu, Binbin Qiu, Donglin Peng, et al. Indirect Current Control Improvement Strategy of Current-mode Pulse-width Modulation Rectifier[J]. Power System Technology, 2012, 36(6): 182-186.

[14] Hulin Liu. Mutual-feed AC Drive Test System Design[D]: Southwest Jiaotong University, 2017.

[15] Ronghai Qu, Chuan Qin. Development Status and Prospects of Electric Vehicles and Their Drive Motors[J]. Southern Power System Technology, 2016, (3): 82-86.

[16] Jianqiang Liu, Qionglin Zheng, Chaoyong Guo, et al. High-speed EMU Traction Converter Heat Capacity[J]. Transactions of China Electrotechnical Society, 2011,26(10): 205-210.

[17] Wensheng Song, Xiaoyun Feng. Electric Traction AC Drive Control and Modulation Technology[M].Beijing: Science Press, 2014.

[18] Qionglin Zheng. Application of Power Electronics Technology in Electric Locomotives[J]. Power Electronics, 2009, (6): 18-24.

[19] Zhian Yan, Xinyi Cui, Shaoping Su. Electromechanics[M].Xi’an: Xi'an Jiaotong University Press,2008.

[20] Ze Xiu. Influence of Power Electronics Technology on the Development of Electric Traction Drive System[J]. Electronic Technology and Software Engineering,2018,(2): 230.

[21] Yunfeng He, Shunhai Wu, Wenguang Chen. Method for Heat Verification and Application of Asynchronous Traction Motor in Subway Train[J]. Electric Locomotives & Mass Transit Vehicles, 2010, (2): 52-54.

[22] Jiagang Cai. Graphical AC Asynchronous Motor Test Technology and Quality Analysis[M].China Electric Power Press,2007.

[23] Xiaoliang Li. Research on Transmission Mode of Diesel Locomotive in China[J]. China Plant Engineering, 2018, (1): 221-222.

[24] Xiaoshang Li. Research on Test System of AC Traction Asynchronous Motor[D]: Beijing Jiaotong University, 2010.

[25] Caodantong Lu, Li Wang. Research and Construction of Joint Test Platform for Traction Electric Drive System[J]. Modern Industrial Economy and Informationization, 2018, (2): 34-36.

[26] H Ochiai, H Nakagami, Y Teranishi, et al. Facility Networking with IP over RS485: Packet Control for Master-slave Cascaded Networks[C]. IEEE International Conference on Smart Grid Communications, 2014.

[27] Wenbin Lei. Profibus and Modbus Protocol Conversion and Its Application in Intelligent Actuator[D]: Nanjing University of Aeronautics,2015.

[28] Ye Li. Fieldbus Technology and Its Application Research[D]: Hunan University, 2002.

[29] Zhonghong Zhao. Research on the Network of AC Traction Monitoring System for Urban Light Rail Transit[D]: Dalian Jiaotong University,2009.

[30] Bo He, Shanmei Cheng, Bo Gong. Research on Single-phase Hybrid Three-level PWM Rectifier[J]. Electrical Automation,2012, (1): 48-51.

[31] Rutian Wang, Youzhi Zeng, Xiaokai Su. Research on Single-phase PWM Rectifier Based on Nonlinear PID Control Theory[J]. Electrical Measurement and Instrumentation, 2017, (10): 113-116.

[32] Jilei Gao, Fei Lin, Qionglin Zheng. Proportional Resonance Control of Single-phase PWM Rectifier Based on Network Pressure Prediction. Transactions of China Electrotechnical Society, 2011,26(5):45-51.

[33] DN Zmood, DG Holmes, GH Bode. Frequency-domain Analysis of Three-phase Linear Current Regulators[J]. IEEE Transactions on Industry Applications, 2001, 37(2):601 -610.

[34] Kai Zhang. Research on Waveform Control Technology of CVCF-PWM Inverter Based on Repetitive Control Theory[D]: Huazhong University of Science and Technology, 2000.

[35] Guofei Teng, Guochun Xiao, Zhibo Zhang, et al. A Single Closed Loop Current Control Strategy of LCL Grid-connected Inverter Using Repetitive Control[J]. Proceedings of the CSEE,2013,(24):13-21.

[36] Yongdong Li, Zedong Li. AC Motor Digital Control System[M].Beijing: Machinery Industry Press, 2016.